Bull Volcanol (2014) 76:772
DOI 10.1007/s00445-013-0772-8

RESEARCH ARTICLE

# Cognate xenoliths in Mt. Etna lavas: witnesses of the high-velocity body beneath the volcano

**Rosa Anna Corsaro · Silvio Giuseppe Rotolo · Ornella Cocina · Gianvito Tumbarello**

Received: 24 May 2013 / Accepted: 12 October 2013


**Abstract** Various xenoliths have been found in lavas of the 1763 ("La Montagnola"), 2001, and 2002–03 eruptions at Mt. Etna whose petrographic evidence and mineral chemistry exclude a mantle origin and clearly point to a cognate nature. Consequently, cognate xenoliths might represent a proxy to infer the nature of the high-velocity body (HVB) imaged beneath the volcano by seismic tomography. Petrography allows us to group the cognate xenoliths as follows: i) gabbros with amphibole and amphibole-bearing mela-gabbros, ii) olivine-bearing leuco-gabbros, iii) leuco-gabbros with amphibole, and iv) Plg-rich leuco gabbros. Geobarometry estimates the crystallization pressure of the cognate xenoliths between 1.9 and 4.1 kbar. The bulk density of the cognate xenoliths varies from 2.6 to 3.0 g/cm$^3$. P wave velocities ($V_P$), calculated in relation to xenolith density, range from 4.9 to 6.1 km/s. The integration of mineralogical, compositional, geobarometric data, and density-dependent $V_P$ with recent literature data on 3D $V_P$ seismic tomography enabled us to formulate the first hypothesis about the nature of the HVB which, in the depth range of 3–13 km b.s.l., is likely made of intrusive gabbroic rocks. These are believed to have formed at the "solidification front", a marginal zone that encompasses a deep region (>5 km b.s.l.) of Mt. Etna's plumbing system, within which magma crystallization takes place. The intrusive rocks were afterwards fragmented and transported as cognate xenoliths by the volatile-rich and fast-ascending magmas of the 1763 "La Montagnola", 2001 and 2002–03 eruptions.

**Keywords** Cognate xenoliths · Gabbro · Geobarometry · Rock density · P-wave velocity · Mt. Etna

Editorial responsibility: G. Giordano

**Electronic supplementary material** The online version of this article (doi:10.1007/s00445-013-0772-8) contains supplementary material, which is available to authorized users.

R. A. Corsaro (✉) · O. Cocina
Istituto Nazionale di Geofisica e Vulcanologia (INGV), Osservatorio Etneo, Sezione di Catania, Piazza Roma, 2, 95125 Catania, Italy
e-mail: corsaro@ct.ingv.it

S. G. Rotolo
Dipartimento di Scienze della Terra e del Mare (DISTeM), Università di Palermo, Via Archirafi, 22, 90123 Palermo, Italy

S. G. Rotolo
Istituto Nazionale di Geofisica e Vulcanologia (INGV), Sezione di Palermo, Via U. La Malfa, 153, 90146 Palermo, Italy

G. Tumbarello
Eni SpA, E&P Division, Via Emilia, 1, San Donato Milanese, 20097 Milan, Italy

Published online: 05 December 2013

## Introduction

The presence of cognate xenoliths in volcanic rocks is quite common in many tectonic settings, such as oceanic ridges, hotspots and subduction zones. Some cognate xenoliths have a mantle or high-pressure origin, while others form in a shallower context (Holness et al. 2007 and references therein). Magmatic xenoliths have also been studied in products of active Italian volcanoes, namely Stromboli (Renzulli and Santi 1997; Mattioli et al. 2003; Laiolo and Cigolini 2006; Corazzato et al. 2008; Tibaldi et al. 2009) and, to a lesser extent, Mt. Etna (Lo Giudice and Ritmann 1975; Aurisicchio and Scribano 1987; Andronico et al. 2005; Corsaro et al. 2007). At Mt. Etna, cognate xenoliths are infrequent and occur exclusively within lavas/pyroclasts of rare eruptions, originally named "eccentric" (Rittmann 1965) and more recently "deep dyke-fed" (DDF, Corsaro et al. 2009b

and references therein). These eruptions are characteristic for a sustained explosive activity at the eruptive vents and produce a phenocryst-poor magma (phenocrysts≤10 vol.%, Armienti et al. 1988; Corsaro et al. 2009b and references therein) that, bypassing the central conduit system, ascends rapidly from a deep storage region of the volcano plumbing system (>5 km b.s.l., Spilliaert et al. 2006). DDF eruptions in historical times occurred in 1763 ("La Montagnola" cone, Fig. 1) (Sturiale 1970; Miraglia 2002), (Bottari et al. 1975; Tanguy and Kieffer 1977; Corsaro et al. 2009b), and 2001 from the Lower Vents (LV, Fig. 1) (Métrich et al. 2004; Viccaro et al. 2006; Corsaro et al. 2007) and in 2002–03 from the Southern Fissures (SF, Fig. 1) (Andronico et al. 2005; Spilliaert et al. 2006; Ferlito et al. 2012).

In many active volcanic systems, such as Hawaii, oceanic ridges (Marsh 2000), Mt. Redoubt, and Mt St. Helens (Okubo et al. 1997; Benz et al. 1996; Lees 1992), the anomalously high values of the P-wave velocity ($V_P$) of sub-volcanic bodies were associated with the presence of intrusive rocks. At Mt. Etna, a high-velocity body (HVB) was imaged by a local earthquake tomography experiment performed by Hirn et al. (1991). The HVB was located S-SE of the summit craters, at a depth of 6 km b.s.l. and embedded in the pre-Etnean sediments. The HVB was imaged in all the following published tomographic analyses, performed either using local earthquake datasets (Cardaci et al. 1993; De Luca et al. 1997; Villaseñor et al. 1998; Chiarabba et al. 2000, 2004; Laigle et al. 2000; Aloisi et al. 2002) or artificial sources (Laigle and Hirn 1999). However, the position and size of the "fast" volume differ in these studies, due to the variation in the consistency and quality of the dataset, the processing method, and also the degree of resolution. Most tomographic studies that have been carried out using local earthquakes imaged the velocity structure beneath the volcano up to about 20 km b.s.l., though showing low resolution at shallow depths.

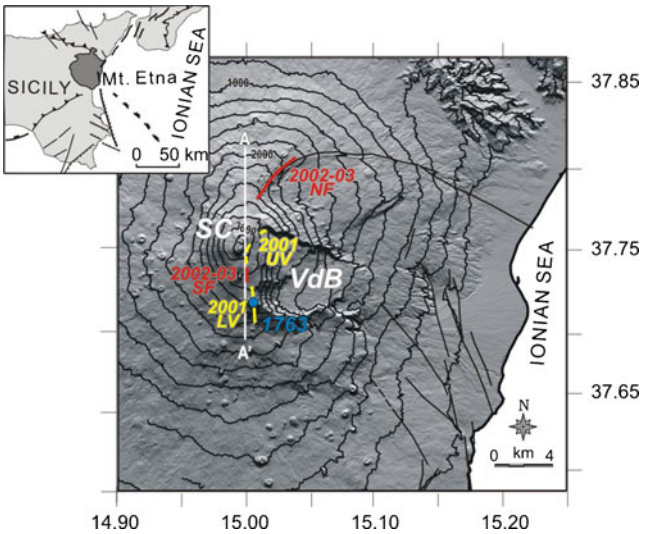


**Fig. 1** Digital Elevation Map of Mt. Etna with its main structural elements. Elevation contour lines are reported at 200-m intervals. The yellow line marks the 2001 Upper (UV) and Lower (LV) Vents; the red line corresponds to the 2002–2003 Northern (NF) and Southern (SF) Fissures. The blue dot represents the scoria cone of the 1763 "La Montagnola" eruption. SC indicates the summit craters. VdB is for Valle del Bove. In the inset, the location of the Mt. Etna volcano and the main regional structural trends are drawn (modified from Barberi et al. 2004). AA' corresponds to the trace of the N-S profile in Figs. 2 and 7

In particular, Chiarabba et al. (2004) imaged a high-velocity body in the S-SE region of the volcano ranging 3–15 km b.s.l., with $V_P$ values between 5.5 and 7.0 km/s. At a greater depth, the high-velocity volume is smaller and is mainly located in the S–SW sector of the volcano. The authors interpreted this anomalous volume as a high-density cumulate body crystallized at depth. Laigle and Hirn (1999), by applying a seismic tomography method with an artificial source, tried to constrain the velocity body at shallow depths and imaged a strong high-velocity anomaly at 2 km b.s.l. Recently, Patanè et al. (2002; 2006) significantly refined the shape of HVB in the shallower layers up to sea level. The 3D-velocity structure computed by Patanè et al. in 2006 (Fig. 2) has been considered as the $V_P$ reference model in this study.

A high-density and highly magnetic body located below the southern part of Valle del Bove (VdB in Fig. 1) was also recognized by Rollin et al. (2000) and Schiavone and Loddo (2007). The time-integrated spatial distribution of the seismicity revealed that the HVB is mainly aseismic. The seismicity encompasses its western and eastern portions, and occasionally is located above its top, testifying to the presence of a brittle region with a high degree of rock-fracturing (Aloisi et al. 2002; Patané et al. 2003; Chiarabba et al. 2004). Recent studies have shed light on the possible role of the HVB in driving the instability phenomena of the eastern portion of the volcano (Allard et al. 2006; Aloisi et al. 2011).

Until now, however, information on the nature of the rocks forming the HVB is lacking. Our study is therefore mainly aimed at understanding whether cognate xenoliths within historical lavas at Mt. Etna might represent fragments of the HVB rooted beneath the volcano. To this end, we studied the cognate xenoliths hosted in lavas of the DDF eruptions occurring in the 1763 "La Montagnola", the 2001 LV and the 2002–03 SF (Fig. 1). We integrated the petro-chemical and physical (density) properties of the cognate xenoliths with the seismological studies. In particular, we investigated their texture, mineralogy, bulk rock major and trace element compositions, and constrained their crystallization pressure by geobarometric methods (Putirka 2008). Furthermore, we calculated the bulk density of the cognate xenoliths and then derived the corresponding P-wave velocities. Finally, we reported the density-dependent $V_P$ values on the 3D-velocity structure provided by the most recent seismic tomography of Patanè et al. (2006) in the depth range 0–15 km b.s.l., to verify if the studied samples may have

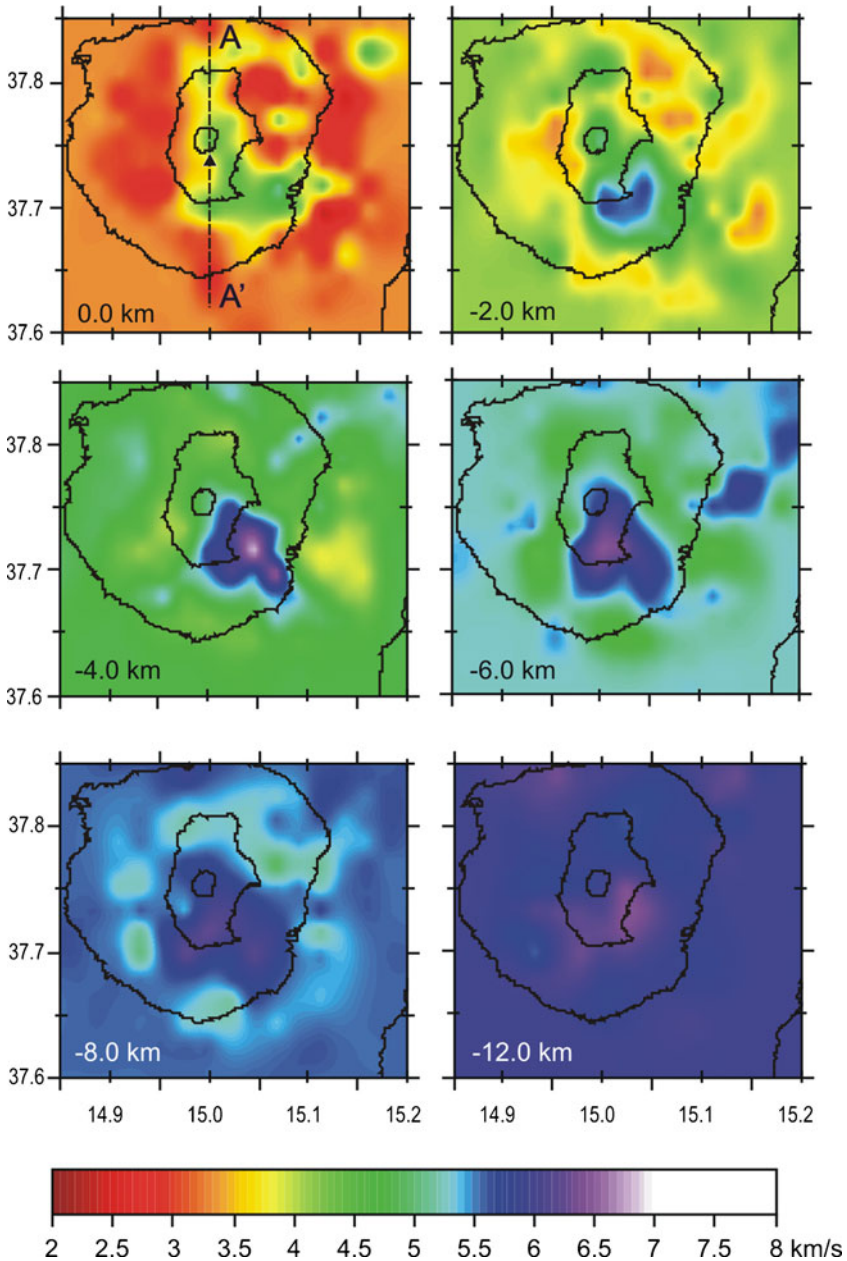


**Fig. 2** Velocity models for $V_P$ (km/s) at six different depth layers ranging from 0 km to 12 km b.s.l, modified from Patanè et al (2006). Coastline and the contour lines of 3,000, 2,000, and 1,000 m are drawn as black lines. The black triangle indicates the center of the inversion grid. AA' marks the trace of the N-S profile in Figs. 1 and 7

originated from magmatic rocks forming the HVB rooted beneath the volcano.

## Sampling and analytical methods

We sampled two cognate xenoliths (1763-INCL and XET) embedded in DDF magma of the 1763 "La Montagnola" eruption. Cognate xenoliths of the 2001 (ZAN200XenB, ZAN200XenC, 2001-INCL) and 2002–03 (281002nodB, 281002C, 02NE05) eruptions were contained in DDF magmas emitted exclusively from eruptive fissures on the southern flank of the volcano, i.e. LV in 2001 and SF in 2002–03 (Fig. 1).

The hand samples vary in size from 1 to 10 cm (Fig. 3) and are all characterized by angular contours without clear evidence of reaction rims at the contact with the host rock (Fig. 3a, b). They are massive, fine to coarse grained, and light to dark colored, depending on the proportion of plagioclase over mafic minerals. Modal analyses have been carried out by counting from 1,800 to 400 points per section, depending on the size of the xenolith, using a squared grid of 0.75 mm. Minerals were analyzed using a JEOL-JXA8200 electron microprobe (EMPA) at INGV Rome. Microprobe analyses were performed using an accelerating voltage of 15 kV, a beam current of 5 nA, and a beam diameter of 1 μm for mineral analyses (see Iezzi et al. 2008 for analytical details). Sodium and potassium were analyzed first to reduce possible

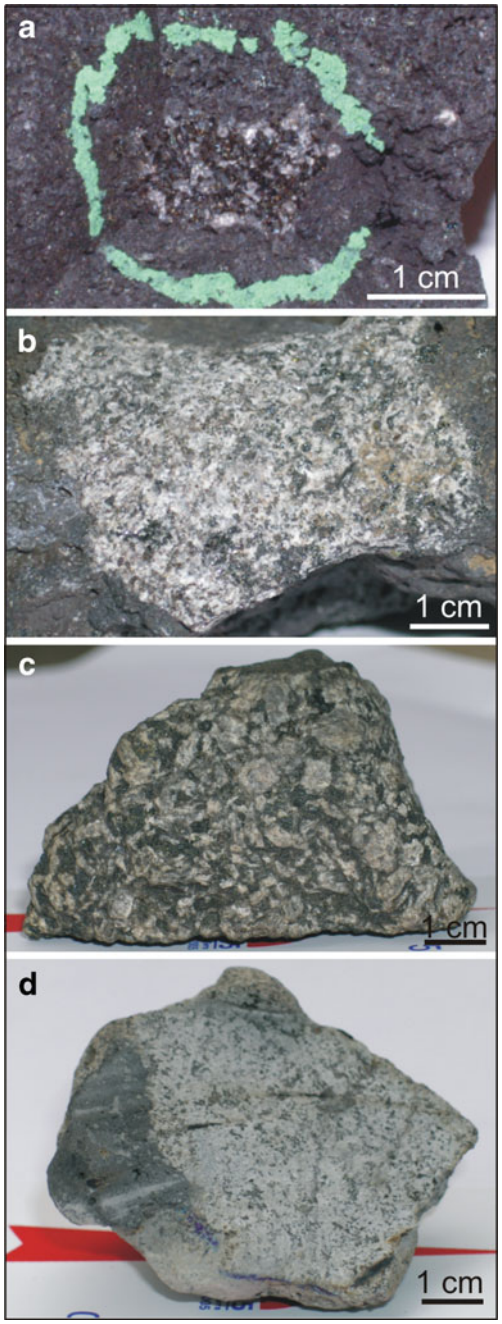


**Fig. 3** Images of hand samples of cognate xenoliths. **a** sample 281002, AMGB group; **b** sample 02NE05, OLLG group; **c** sample 2001-INCL, AMLG group; **d** sample 1763-INCL, PLLG group

volatilization effects. The following standards were adopted: jadeite (Si and Na), corundum (Al), forsterite (Mg), andradite (Fe), rutile (Ti), orthoclase (K), barite (Ba), celestine (Sr), F-phlogopite (F), apatite (P), spessartine (Mn), metals (Cr). ZAF correction was used. The standard deviation (1σ) in weight percent (wt. %) is 0.34 for $SiO_2$, 0.06 for $TiO_2$, 0.11 for $Al_2O_3$, 0.10 for FeO, 0.03 for MnO, 0.07 for MgO, 0.16 for CaO, 0.05 for $Na_2O$, 0.03 for $K_2O$, 0.04 for $P_2O_5$.

Only three cognate xenoliths (1763INCL, 2001-INCL and 02NE05) were large enough to be extracted from the host lava. Their bulk rock compositions of major and trace elements were measured respectively with inductively coupled plasma optical emission spectroscopy (ICP-OES) and inductively coupled plasma mass spectrometry (ICP-MS) at the Centre de Recherches Pétrographiques et Géochimiques (SARM) in Nancy (France). Analytical uncertainty (1σ) was: <1 % for $SiO_2$ and $Al_2O_3$, <2 % for $Fe_2O_3$, MgO, CaO, $Na_2O$, $K_2O$, < 5 % for MnO, and $TiO_2$, 5–10 % for $P_2O_5$, and between 5 and 10 % for all trace elements, except for Ni (>25 %).

The direct density measurements of the XET and 2001-INCL cognate xenoliths were carried out with an electronic semi-microbalance Sartorius equipped to measure the density of a solid sample by applying the Archimedean principle. The hydrostatic balance enables the solids to be weighed in air (Wa), as well as in water (Wl), and to measure its density ($\rho_S$) if the density of the liquid ($\rho_l$=1 g/cm$^3$ using distilled water) is known: $\rho_S = Wa \times \rho_l/(Wa\text{-}Wl)$.

## Petrography, mineralogy and bulk rock chemistry

Cognate xenoliths were classified according to the criteria of Le Maitre (2002) for plutonic rocks. All the samples belong to the gabbro group and, depending on the 'color index', have been subdivided into 'leuco-'and 'mela-gabbro' groups. We used the qualifier 'Plg-rich' gabbros for two samples (1763-INCL and XET), essentially made up of plagioclase and accessory biotite and Fe-Ti oxides. If the modal abundance of a mineral other than plg, cpx and oxide is higher than 10 %, we named the rock 'mineral-bearing' gabbro. If lower than 10 %, the rock was classified as gabbro 'with mineral'.

In the following description, we report the petrographic features of the cognate xenoliths divided into four main groups, according to their modal mineralogy (Table 1). Mineral compositions are expressed as variation ranges or mean values, both resulting from of at least five EMPA analyses.

(1a) **Gabbros with amphibole (AMGB)** and (1b) **amphibole-bearing mela-gabbros (AMMG)**, embedded in 2001 and 2002–03 lavas. Both groups are comprised of: Ca-rich plagioclase (on 15 phenocryst analyses, core = $An_{90–67}$, rim = $An_{86–49}$), salitic clinopyroxene (core = $Wo_{44–47}En_{41–44}Fs_{12–13}$, rim = $Wo_{45–49}En_{35–44}Fs_{10–16}$) olivine (unzoned: core = $Fo_{75.8}$, rim = $Fo_{75.6}$) and Ca-amphibole (Mg-hastingsite, Leake et al. 1997) (Table A supplementary material). Amphibole is coarse-grained (≤1 cm), chemically unzoned, and forms a unique poikilitic mass hosting: euhedral plagioclase (to 2 mm in length), subhedral clinopyroxene (up to 3-mm long), and fewer anhedral olivine grains. The Ti apfu content

**Table 1** Mineral abundances (vol. %) of the cognate xenoliths. Analyses are recalculated to 100 %, void–free, after subtracting glass and breakdown corona products

| Sample | 281002nodB | ZAN2001XenB | ZAN2001XenC | 281002C | 02NE05a | 02NE05b | 2001-INCLa | 2001-INCLb | 1763-INCL | XET |
|---|---|---|---|---|---|---|---|---|---|---|
| Group | AMGB | AMMG | AMMG | AMMG | OLLG | OLLG | AMLG | AMLG | PLLG | PLLG |
| Host lava | 2002-03 | 2001 | 2001 | 2002-03 | 2002-03 | 2002-03 | 2001 | 2001 | 1763 | 1763 |
| Plg | 43 | 26 | 18 | 26 | 65 | 61 | 70 | 71 | 87 | 85 |
| Cpx | 35 | 14 | 14 | 35 | 19 | 19 | 13 | 20 | tr. | 0 |
| Ol | 4 | 3 | 2 | 2 | 12 | 13 | 5 | 2 | 0 | 0 |
| Bt | 0 | 0 | 0 | 0 | 0 | 0 | tr. | tr. | 6 | 8 |
| Amph | 2 | 51 | 63 | 30 | 0 | 0 | 4 | 2 | 0 | 0 |
| Ox | 16 | 6 | 3 | 7 | 4 | 7 | 8 | 5 | 7 | 7 |

02NE05a and 02NE05b are two thin sections of the sample 02NE05, as well as 2001-INCLa and 2001-INCLb of sample 2001-INCL

*Plg* plagioclase, *Cpx* clinopyroxene, *Ol* olivine, *Bt* biotite, *Amph* Amphibole, *Ox* oxide. tr. is for trace amounts

(on a 13 cations basis) is in the range 0.40–0.49, and the Mg/(Mg + Fe) varies from 0.69 to 0.71.

Amphibole is characterized by frequent breakdown coronas (Fig. 4a), due to the instability during xenolith ascent, consisting of clinopyroxene (fassaite/salite), rhönite (Table B supplementary material), plagioclase and magnetite (Fig. 4b). Ti-magnetite composition is ulvospinel ($Usp_{35}$). Mineral compositions in AMGB and AMMG cognate xenoliths overlap the compositional field described by Clocchiatti et al. (2004), Corsaro et al. (2007), and Viccaro et al. (2007) for cognate xenoliths in 2001 lavas.

(2) **Olivine-bearing leuco-gabbros (OLLG)**. These cognate xenoliths are medium-grained (maximum length ≤4 mm) and were found in 2002–03 SF lavas. In order of decreasing abundance, they are made up of plagioclase (phenocryst composition in the range: core = $An_{84–87}$, rim = $An_{52–62}$), clinopyroxene (salitic in composition, core = $Wo_{45–47}En_{40–41}Fs_{12–15}$, rim = $Wo_{45–47}En_{39–40}Fs_{13–15}$), olivine (core = $Fo_{71.3}$, rim = $Fo_{71.2}$) and Ti-magnetite, with a rather high ulvospinel component, up to 46 mol %. Minerals are arranged without a preferred orientation (Fig. 4c), with euhedral to subhedral olivine (to 2 mm in length) often included in subhedral clinopyroxene (up to 3 mm in size), while subhedral plagioclase (to 4-mm long) is a late-crystallizing phase.

(3) **Leuco-gabbros with amphibole (AMLG)**. This group includes cognate xenoliths from the 2001 eruption. The mineral assemblage is: plagioclase (core = $An_{70–79}$, rim = $An_{50–55}$), clinopyroxene (core = $Wo_{44–45}En_{41–44}Fs_{12–13}$, rim = $Wo_{43–46}En_{41–45}Fs_{12–13}$), olivine (core = $Fo_{75.4}$. rim = $Fo_{75.8}$), Ti-magnetite ($Usp_{39}$) and Mg-hastingsite, with Ti (apfu) =0.44–0.52 and the Mg/(Mg + Fe) in the range 0.69–0.71 (Table A supplementary material). Noteworthy is the occurrence of biotite (Fig. 4d) with mean $TiO_2$ = 6.2 wt.% and XMg (=Mg/(Mg + $Fe_{tot}$)) =0.67–0.72. Biotite is very rare in Mt. Etna xenoliths, only found in trace amounts. These cognate xenoliths are the coarsest in grain size among those studied (plagioclase is up to 8-mm long). Textural relationships suggest that: i) plagioclase, largely the most abundant mineral phase, is strongly oriented and is euhedral with respect to the intercumulus clinopyroxene; ii) amphibole (whose maximum length reaches 3 mm) is a late-crystallizing phase: it almost entirely fills a former magma cavity, leaving only small glass remnants (Fig. 4e). More rarely, amphibole envelops deeply lobate clinopyroxene and biotite. Interstitial Ti-magnetite occurs mostly within melt pools in large crystals (up to 3 mm), or more rarely is included in clinopyroxene. Apatite and pyrite occur in accessory amounts.

(4) **Plg-rich leuco gabbros (PLLG)**. These cognate xenoliths were found in products of the 1763 eruption. They consist almost exclusively of plagioclase (Fig. 4f), as long as 2 mm, which is consistently zoned (core=$An_{52–64}$, rim=$An_{2–43}$) and arranged in unoriented interlocking texture; interstitial plagioclase is Ca-poor ($An_{1–26}$). Biotite (8 vol.%, Table 1) is up to 1 mm in length and fills the interstices among plagioclase laths. These plagioclase compositions are rather Ca-poor if compared to plagioclase crystals inferred to have grown at high depths in the Etna plumbing system, whose composition and texture reflect the complex interplay of temperature, ascent rates and $H_2O$-melt gradients (Viccaro et al. 2010; Nicotra and Viccaro 2012). Biotite, 1–2 mm in size, is characterized by a mean $TiO_2$ content=5.3 wt.% and an average XMg of 0.63 that is lower than the biotite of AMLG group. Clinopyroxene occurs in trace amounts and is rather Fe-rich ($Wo_{47}En_{17}Fs_{36}$). Ti-magnetite ($Usp_{42}$) is fairly abundant (7 vol.%), with a maximum size of 500 μm; it occurs either as inclusions in plagioclase or in interstitial positions among plagioclase phenocrysts.

Bulk rock major and trace element compositions have been measured (Table 2) in three cognate xenoliths,

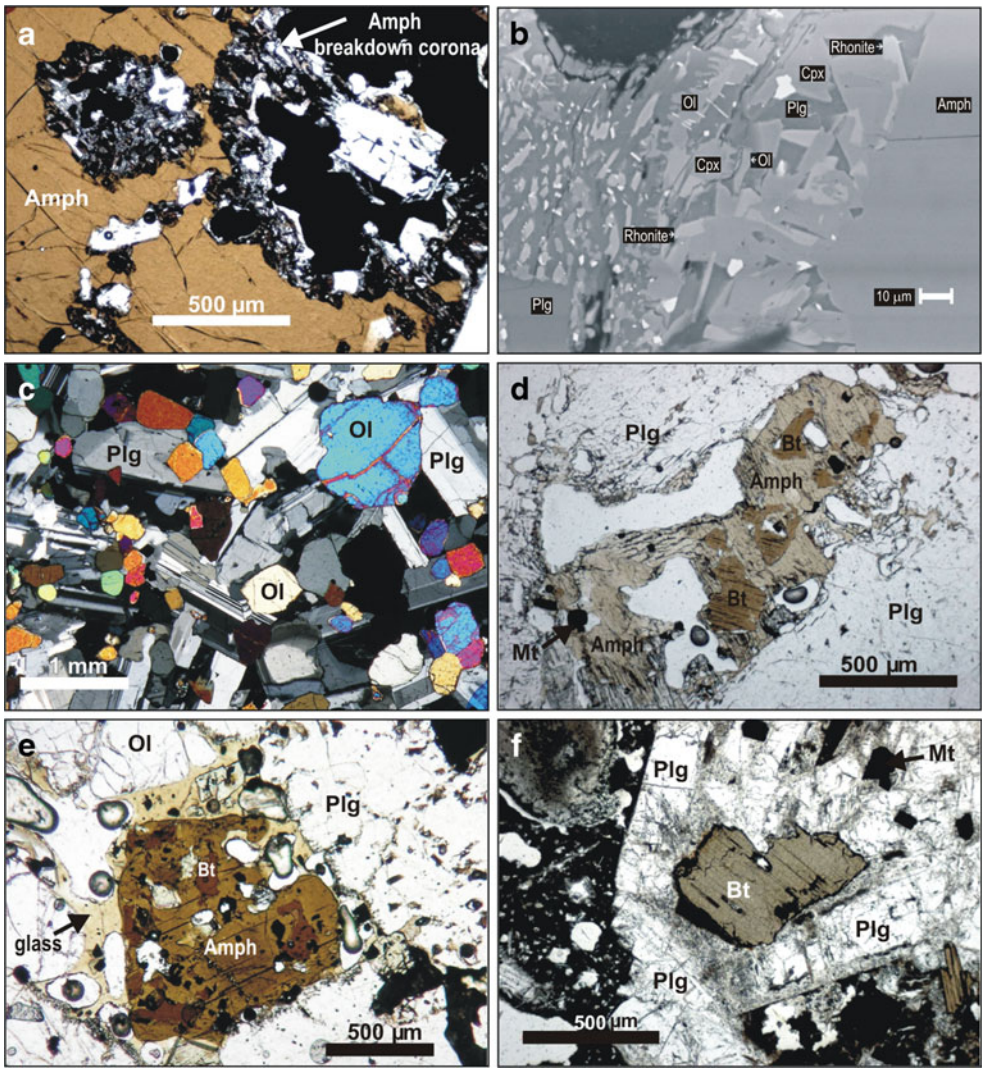


**Fig. 4** **a** Microphoto of an amphibole (Amph) breakdown corona in the AMMG group (sample ZAN2001XenB). Parallel Nicols; **b** BSE image of amphibole breakdown rim in the AMMG group (sample ZAN2001XenC), showing the radial growth of rhönite, olivine, clinopyroxene at the expense of amphibole; **c** Texture of sample 02NE05b (OLLG group) with evident plagioclase (Plg) and clinopyroxene (Cpx). Crossed Nicols; **d** Microphoto of plagioclase, amphibole and biotite (Bt) in the AMLG group (sample 2001-INCLa). Parallel Nicols; **e** amphibole enclosing biotite almost entirely fills a former glass pool in the AMLG group (sample 2001-INCLb). Parallel Nicols; **f** Microphoto of plagioclase and biotite phenocrysts in the PLLG group (sample 1763-INCL). Parallel Nicols

namely 1763-INCL, 2001-INCL and 02NE05, belonging respectively to the PLLG, AMLG and OLLG groups. Data have been plotted (Fig. 5) in the TAS grid (Le Maitre 2002) and in diagrams between selected trace elements (Fig. 6), to compare xenoliths to each other and to their host trachybasaltic lavas (average composition of 1763, 2001 and 2002–03 DDF magmas in Table 2 are respectively from: Corsaro et al. 2009b; Corsaro et al. 2007; Corsaro et al. 2009a). The compositions of the 1763, 2001 and 2002–03 hosting DDF lavas are very homogeneous, unlike the cognate xenoliths, which are highly variable, ranging from 44.55 to 51.41 $SiO_2$ wt.% and from 2.67 to 6.95 $Na_2O + K_2O$ wt. %. The OLLG is the most primitive group, as evidenced by the low content of $SiO_2$, alkali (Fig. 5) and incompatible trace elements (Th, Rb, Cs, La, Yb,), and by the abundance of compatible trace elements such as Co, Cr, Ni and V (Fig. 6 and Table 2). AMLG and PLLG are more evolved since they show higher silica, alkali, incompatible trace elements and lesser compatible ones. On the whole, there are evident compositional differences between the cognate xenoliths and respective host rocks (Figs. 5, 6 and Table 2).

## Constraints on temperature and pressure of crystallization of the cognate xenoliths

During Mt. Etna's lifetime, amphibole occurrence has been limited to the most evolved magmas (mugearite, benmoreite) erupted from the Timpe to Ellittico phases, about 220–15 ka (Corsaro et al. 2007), whereas it is not found in the more mafic and younger than 15 ka products, except for the 2001 eruption (Clocchiatti et al. 2004; Corsaro et al. 2007; Viccaro et al. 2007).

Although there are few experimental constraints for amphibole stability in alkaline mafic magmas (e.g., Barclay

**Table 2** Bulk rock major and trace elements of selected cognate xenoliths (1763-INCL, 2001-INCL and 02NE05)

| Sample | 1763-INCL | 1763 lava average [a] ($n$=3) | 2001-INCL | 2001 lava average ($n$=12) | 02NE05 | 2002-03 lava average ($n$=18) |
|---|---|---|---|---|---|---|
| Group | PLLG | | AMLG | | OLLG | |
| Type | XENOLITH | HOST LAVA | XENOLITH | HOST LAVA | XENOLITH | HOST LAVA |
| $SiO_2$ | 51.41 | 47.27 | 47.64 | 47.33 | 44.55 | 47.31 |
| $TiO_2$ | 1.18 | 1.62 | 1.34 | 1.63 | 1.18 | 1.67 |
| $Al_2O_3$ | 19.51 | 16.69 | 22.27 | 16.67 | 17.85 | 16.71 |
| $Fe_2O_3$ | 1.29 | 1.76 | 1.40 | 1.75 | 1.99 | 1.75 |
| FeO | 6.46 | 8.80 | 7.02 | 8.77 | 9.93 | 8.74 |
| MnO | 0.19 | 0.18 | 0.13 | 0.17 | 0.18 | 0.17 |
| MgO | 3.34 | 6.30 | 3.18 | 6.24 | 9.76 | 6.36 |
| CaO | 6.56 | 10.94 | 11.73 | 10.94 | 11.11 | 10.91 |
| $Na_2O$ | 4.97 | 3.39 | 3.76 | 3.35 | 2.21 | 3.30 |
| $K_2O$ | 1.98 | 1.34 | 0.58 | 1.89 | 0.46 | 1.93 |
| $P_2O_5$ | 0.71 | 0.50 | 0.79 | 0.48 | 0.13 | 0.48 |
| L.O.I. | 1.62 | 0.86 | 0.76 | 0.77 | 0.81 | 0.66 |
| Tot | 99.20 | 99.65 | 100.59 | 99.98 | 100.15 | 99.99 |
| [b]Mg# | 0.44 | 0.52 | 0.41 | 0.52 | 0.60 | 0.52 |
| Rb | 48.6 | 26.5 | 8.4 | 45.1 | 7.7 | 46.6 |
| Cs | 0.61 | 0.48 | 0.20 | 0.92 | 0.18 | 0.86 |
| Sr | 1,331 | 1,065 | 2,179 | 1,085 | 1,276 | 1,063 |
| Ba | 893 | 552 | 455 | 566 | 268 | 560 |
| Ta | 4.74 | 2.40 | 1.09 | 2.38 | 0.53 | 2.34 |
| Th | 15.25 | 7.04 | 3.81 | 7.56 | 1.59 | 6.89 |
| U | 4.76 | 1.98 | 1.04 | 2.21 | 0.44 | 1.99 |
| Zr | 309 | 182 | 69 | 196 | 52 | 195 |
| Hf | 5.63 | 4.00 | 1.70 | 4.35 | 1.42 | 4.38 |
| Nb | 82.0 | 41.6 | 18.6 | 38.9 | 8.4 | 38.6 |
| La | 102.7 | 53.1 | 48.3 | 52.5 | 15.5 | 51.3 |
| Ce | 179.7 | 99.9 | 90.9 | 101.4 | 29.8 | 99.6 |
| Nd | 66.1 | 44.3 | 39.4 | 45.1 | 14.3 | 44.8 |
| Sm | 10.62 | 8.22 | 6.91 | 8.88 | 2.97 | 8.77 |
| Eu | 3.09 | 2.49 | 2.50 | 2.66 | 1.20 | 2.67 |
| Tb | 1.05 | 0.90 | 0.66 | 0.97 | 0.34 | 1.00 |
| Yb | 2.29 | 1.93 | 1.14 | 2.05 | 0.70 | 2.11 |
| Lu | 0.36 | 0.29 | 0.16 | 0.33 | 0.10 | 0.31 |
| Y | 27.4 | 23.5 | 15.4 | 25.6 | 8.6 | 25.8 |
| Ni | 11.7 | 35.7 | 8.0 | 30.4 | 68.8 | 37.7 |
| Cr | 8.2 | 56.2 | 5.6 | 64.7 | 102.0 | 57.2 |
| V | 162 | 300 | 202 | 300 | 296 | 299 |
| Co | 21.1 | 41.0 | 25.0 | 41.6 | 66.4 | 41.2 |
| Cu | 121.2 | 128.4 | 0.20 | 0.92 | 26.4 | 131.2 |

The compositions of the host lavas are averaged from literature: 1763 (Corsaro et al. 2009b), 2001 (Corsaro et al. 2007), 2002–03 (Corsaro et al. 2009a)

[a] $n$ number of analyses

[b] Mg# = $(Mg/(Mg + Fe^{2+})$ moles, assuming $Fe^{3+}/Fe^{2+} = 0.2$

and Carmichael 2004; Pompilio and Rutherford 2002), they concur in fixing the upper thermal stability at around 1,030 °C for $P_{H2O}$<3 kbar, to 1,000 °C with decreasing pressure.

Amphibole breakdown products include: rhönite + clinopyroxene + plagioclase ± melt ± olivine (Grapes et al. 2003; Alletti et al. 2005).

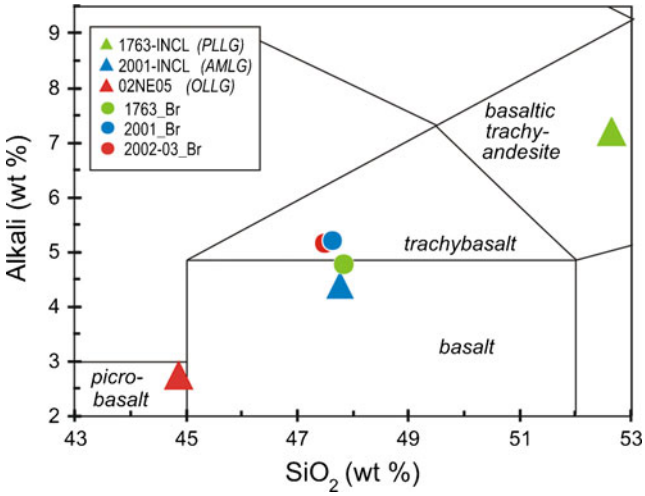


**Fig. 5** TAS diagram (Le Maitre 2002) showing bulk rock compositions of cognate xenoliths (1763-INCL, 2001-INCL, 02NE05) and the average of the respective 1763, 2001 and 2002–03 host lavas (data are respectively from: Corsaro et al. 2009b; Corsaro et al. 2007; Corsaro et al. 2009a). In the legend, "Br" is for "Bulk rock"

According to Kunzmann (1989), for rhönite to crystallize under magmatic conditions, a pressure below 0.6 kbar is required, along with a temperature between 840 °C and 1200 °C. Huckenholz et al. (1988) determined the stability field for the coexistence of rhönite and amphibole in an even narrower range of temperature and pressure: between 0.5 kbar, 1,050 °C and 0.2 kbar, 1,000 °C. Huckenholz et al. (1988) state that basaltic amphibole upon decompression breaks down into rhönite + plagioclase at low pressure (below 0.5 kbar) and relatively high temperature (1,050–1,140 °C). In any case, Mt. Etna lava temperatures (1,070–1,110 °C, Corsaro and Pompilio 2004a) are considerably above the upper thermal stability limit of amphibole (Barclay and Carmichael 2004; Pompilio and Rutherford 2002), and thus strongly suggest a xenocrystic origin of amphibole and/or their provenance from colder/wetter portions (roof, walls) of the magmatic reservoir (Corsaro et al. 2007), or else crystallization in a closed reservoir under overpressure conditions (Viccaro et al. 2007) .

The pressure of crystallization of the cognate xenoliths was calculated using the Putirka (2008) clinopyroxene-liquid geothermobarometer (Eq. 32a and 32c in Putirka 2008). As for criteria for the chemical equilibrium between clinopyroxene and liquid, we selected only crystals (Table 3) whose $KD_{Fe\text{-}Mg}^{cpx\text{-}liq}$ (i.e., Fe/Mg in cpx)/(Fe/Mg in liquid) was in the range of values considered to represent crystal-liquid equilibrium (0.27±0.03, Putirka 2008), taking the bulk rock analyses of the hosting lavas as representative of the liquid (an assumption supported by their low phenocryst content) and fixing a temperature of 1,080 °C consistent with present-day temperatures of Mt. Etna lavas, (Corsaro and Pompilio 2004a). The results, according to Eq. 32a of Putirka (2008) are reported in Table 3, and can be summarized as follows:

- the AMGB group is characterized by the highest pressure from 4.1 to 2.1 kbar, the lower value resulting from rim analyses;
- the AMMG group shows intermediate pressure values in the range 2.3–4.1 kbar (core analyses) and 2.6–3.1 kbar (rim analyses).
- The AMLG group show the lowest P values, at 1.9–2.5 kbar (core analyses) and 3.2 (rim analysis).
- OLLG clinopyroxenes were not considered because their $KD_{Fe\text{-}Mg}^{cpx\text{-}liq}$ was in the range 0.36–0.41, well above the equilibrium value.

The cognate xenoliths therefore crystallized in a pressure range that, following Putirka (2008), is comprised between 1.9 and 4.1 kbar. It corresponds to a depth range of 4–13 km b.s.l., assuming the crustal stratigraphy and density of Mt. Etna's basement as determined by Corsaro and Pompilio (2004b), with the AMMG and AMGB enclaves being the deepest. Therefore, the cognate xenoliths might represent fragments of intrusive magmatic rocks that crystallized beneath the volcano in a depth range of 4–13 km.

## Calculation of xenolith densities and derived P-wave velocity

Most samples were too small to be extracted from the host rock, so the xenolith densities were calculated with an approach described below. Firstly, for each group (Table 4) we took into account the density (http://webmineral.com) of the component minerals ($\rho_M$, Table 4) and the average mineral abundances (Table 4, values are averaged from Table 1). For solid solutions (plagioclase, olivine, clinopyroxene, biotite and Ti-magnetite), the weight proportions of the end-members were considered for calculations of $\rho_M$ (see examples in the footnote[a] of Table 4); for amphibole, the density of Mg-hastingsite (=3.12 g/cm$^3$) has been envisaged. The average mineral abundances (vol. %) were converted in average mineral weights (wt.%, $W_M$ Table 4). The density of a group ($\rho_C$) was then calculated from $\rho_M$ and $W_M$ (Table 4):

$$\rho_C = \frac{\left(\sum_{i=1}^{n} W_M\, \rho_M\right)}{100}$$

For example (see Table 4), for the PLLG group consisting of 81 % plagioclase ($An_{54}$), 12 % Ti-mt ($Usp_{42}$) and 7 % biotite, $\rho_C$=[(2.68×81)+(4.92×12)+(2.94×7)]/100=3.0 g/cm$^3$.

The calculated $\rho_C$ ranges from 3.0 g/cm$^3$ for PLLG to 3.4 g/cm$^3$ for AMGB (Table 4).

This approach, however, does not take into account that the actual bulk density of a rock also depends on the presence of voids and trapped fluids, as well as any modification induced by temperature/pressure effects at depth. To evaluate the

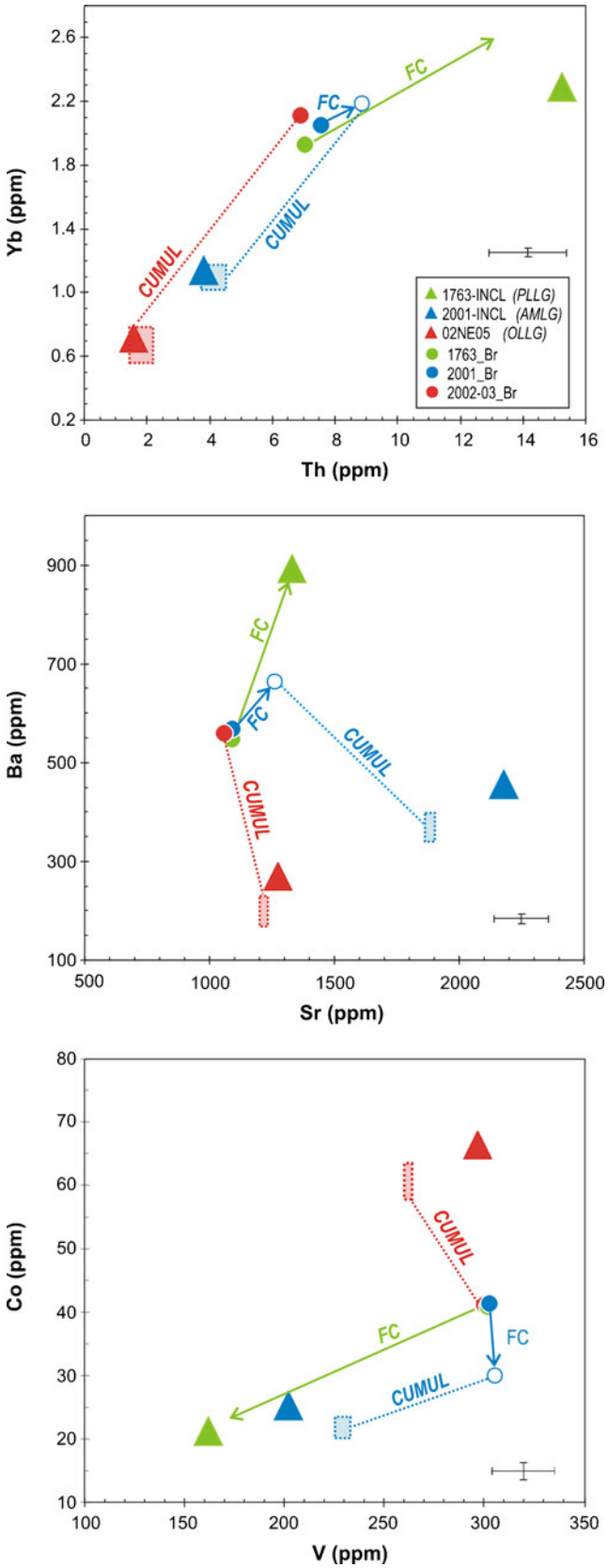


**Fig. 6** Binary diagrams with selected trace elements for bulk rock composition of cognate xenoliths (1763-INCL, 2001-INCL, 02NE05) and the average of the 1763, 2001 and 2002–03 host lavas (data are respectively from: Corsaro et al. 2009b; Corsaro et al. 2007; Corsaro et al. 2009a). In the legend, "Br" is for "Bulk rock". FC pattern (*green arrow*) links the 1763 lavas with the residual magma resulting from the crystallization of 46 % Plg, Ol, Cpx and Ti-mt (see Section "The formation of the cognate xenolith hosted in 1763 lavas" for details). FC pattern (*blue arrow*) links the parental 2001 host lava with the residual magma (symbol: *open blue circle*) resulting from the crystallization of 10 % Cpx and 5 % Ol (see Section "The formation of the cognate xenolith hosted in 2001 and 2002–03 lavas" for details). The CUMUL pattern (*dotted red line*) links the 2002–03 host lava with the range of cumulitic compositions (*red-colored rectangle*) modeled for the addition of Plg, Ol, Cpx, Ti-mt (see Section "The formation of the cognate xenolith hosted in 2001 and 2002–03 lavas") to the 2002–03 magma. The CUMUL pattern (*dotted blue line*) links the residual magma fractionated from 2001 host lava (symbol: *open blue circle*) with the range of cumulitic compositions (*blue-colored rectangle*) modeled for the addition of Plg, Cpx, Ti-mt and Ol (see Section "The formation of the cognate xenolith hosted in 2001 and 2002–03 lavas")

contribution of these factors, we performed direct density measurements on the two mineable cognate xenoliths (Table 5, see also Section "Sampling and analytical methods" for details), and assumed that the difference between the calculated ($\rho_C$) and the measured density ($\rho_S$, see Table 5) in some ways takes the contribution of the above factors into account. The average $\rho_S$ values are 2.59±0.03 (1σ) for XET and 2.62±0.01 g/cm$^3$ for 2001-INCL (Table 5), resulting in 0.4 g/cm$^3$ lower than the respective $\rho_C$. Consequently, we decreased the $\rho_C$ by 0.4 g/cm$^3$, to finally derive the bulk density of each group, whose values ranged from 2.6 g/cm$^3$ for PLLG to 3.0 g/cm$^3$ for AMGB (Table 4).

Once the bulk density of different groups was determined, we then derived the corresponding P-wave velocities following the model of Gebrande et al. (1982) (see also, Kozlovskaya et al. 2004) that proved reliable for large-scale igneous bodies:

$$V_P[\mathrm{km/s}] = \left(2.82 \times \rho\left[\mathrm{g/cm^3}\right]\right) - 2.37 \pm 0.18$$

As a result, we obtained $V_P$ values ranging from 4.9±0.18 for PLLG to 6.1±0.18 km/s for AMGB (Table 4).

To constrain the vertical distribution of the calculated $V_P$ inside the volcanic basement, we reported them on an N-S vertical section (see trace AA' in Fig. 2) derived from the Patanè et al. (2006) velocity model, in the depth range 0–15 km b.s.l. (Fig. 7). Referring to a vertical direction under the summit craters (vertical yellow line in Fig. 7), the calculated $V_P$ values (from 4.9 to 6.1 km/s), extend in the depth range 3–12 km b.s.l. inside the HVB. In other words, the density-dependent $V_P$ of the studied cognate xenoliths coincide with $V_P$ provided by seismic tomography in the depth range 3–12 km b.s.l. By integrating these results with the depth range (4–13 km b.s.l.) provided by geobarometric calculations (see Section "Constraints on temperature and pressure of crystallization of the cognate xenoliths"), we may therefore conclude

**Table 3** Representative clinopyroxene analyses and geobarometric calculations

| Sample | 281002 nodB | | ZAN2001xenB | | | | ZAN 2001xenC | | | | | 2001-INCL | | | | |
|---|---|---|---|---|---|---|---|---|---|---|---|---|---|---|---|---|
| Group | AMGB | | AMMG | | | | AMMG | | | | | AMLG | | | | |
| Label | Core | Rim | Core | Core | Core | Core | Rim | Rim | Rim | Rim | Rim | Core | Core | Core | Core | Rim |
| N° spot | 36 | 37 | 37 | 43 | 45 | 49 | 38 | 44 | 46 | 48 | 50 | 28 | 30 | 55 | 63 | 47 |
| $SiO_2$ | 50.29 | 50.06 | 52.58 | 50.20 | 50.23 | 50.75 | 51.67 | 51.16 | 50.94 | 49.85 | 49.66 | 51.31 | 51.26 | 52.53 | 51.13 | 50.97 |
| $TiO_2$ | 0.99 | 1.28 | 0.67 | 1.24 | 1.33 | 1.09 | 1.01 | 1.06 | 1.15 | 1.07 | 1.37 | 0.96 | 0.82 | 0.81 | 1.14 | 0.69 |
| $Al_2O_3$ | 4.77 | 4.29 | 2.50 | 4.50 | 4.77 | 4.43 | 3.47 | 4.10 | 4.24 | 4.52 | 5.15 | 3.15 | 3.32 | 2.32 | 3.16 | 3.03 |
| $FeO_{tot}$ | 7.26 | 6.92 | 7.26 | 7.10 | 6.88 | 6.98 | 7.26 | 6.83 | 6.81 | 6.86 | 6.73 | 7.33 | 7.00 | 7.10 | 7.14 | 7.03 |
| MnO | 0.22 | 0.13 | 0.31 | 0.22 | 0.19 | 0.21 | 0.21 | 0.26 | 0.19 | 0.21 | 0.14 | 0.37 | 0.21 | 0.38 | 0.35 | 0.41 |
| MgO | 15.22 | 15.19 | 15.60 | 14.78 | 14.21 | 14.69 | 15.08 | 14.73 | 15.01 | 14.66 | 14.30 | 15.31 | 15.34 | 15.07 | 14.94 | 15.27 |
| CaO | 21.10 | 21.70 | 21.30 | 21.94 | 21.85 | 22.05 | 21.62 | 21.98 | 22.15 | 22.21 | 22.66 | 21.40 | 21.93 | 21.69 | 21.38 | 20.66 |
| $Na_2O$ | 0.45 | 0.37 | 0.53 | 0.47 | 0.49 | 0.45 | 0.49 | 0.43 | 0.34 | 0.48 | 0.36 | 0.48 | 0.50 | 0.66 | 0.50 | 0.54 |
| $K_2O$ | 0.00 | 0.02 | 0.00 | 0.00 | 0.00 | 0.00 | 0.00 | 0.00 | 0.00 | 0.01 | 0.00 | 0.01 | 0.01 | 0.01 | 0.00 | 0.04 |
| $Cr_2O_3$ | 0.00 | 0.02 | 0.00 | 0.00 | 0.00 | 0.00 | 0.00 | 0.01 | 0.01 | 0.03 | 0.00 | 0.00 | 0.00 | 0.00 | 0.00 | 0.01 |
| Total | 100.29 | 99.95 | 100.73 | 100.46 | 99.95 | 100.66 | 100.80 | 100.57 | 100.84 | 99.90 | 100.35 | 100.31 | 100.38 | 100.56 | 99.72 | 98.66 |
| Cations p.f.u. on a six oxygen basis | | | | | | | | | | | | | | | | |
| Si | 1.857 | 1.856 | 1.930 | 1.855 | 1.862 | 1.869 | 1.898 | 1.883 | 1.870 | 1.853 | 1.837 | 1.897 | 1.893 | 1.934 | 1.900 | 1.911 |
| Ti | 0.027 | 0.036 | 0.019 | 0.035 | 0.037 | 0.030 | 0.028 | 0.029 | 0.032 | 0.030 | 0.038 | 0.027 | 0.023 | 0.022 | 0.032 | 0.020 |
| Al (IV) | 0.143 | 0.144 | 0.070 | 0.145 | 0.138 | 0.131 | 0.102 | 0.117 | 0.130 | 0.147 | 0.163 | 0.103 | 0.107 | 0.066 | 0.100 | 0.089 |
| Al (VI) | 0.065 | 0.044 | 0.037 | 0.051 | 0.070 | 0.061 | 0.048 | 0.060 | 0.054 | 0.052 | 0.062 | 0.034 | 0.037 | 0.035 | 0.038 | 0.045 |
| Fe | 0.224 | 0.214 | 0.223 | 0.219 | 0.213 | 0.215 | 0.223 | 0.210 | 0.209 | 0.213 | 0.208 | 0.227 | 0.216 | 0.219 | 0.222 | 0.220 |
| Mn | 0.007 | 0.004 | 0.010 | 0.007 | 0.006 | 0.007 | 0.007 | 0.008 | 0.006 | 0.006 | 0.004 | 0.011 | 0.006 | 0.012 | 0.011 | 0.013 |
| Mg | 0.838 | 0.840 | 0.853 | 0.814 | 0.785 | 0.806 | 0.826 | 0.808 | 0.821 | 0.813 | 0.789 | 0.844 | 0.845 | 0.827 | 0.828 | 0.853 |
| Ca | 0.835 | 0.862 | 0.838 | 0.869 | 0.868 | 0.870 | 0.851 | 0.867 | 0.871 | 0.885 | 0.898 | 0.847 | 0.868 | 0.856 | 0.851 | 0.830 |
| Na | 0.032 | 0.027 | 0.038 | 0.034 | 0.035 | 0.032 | 0.035 | 0.031 | 0.024 | 0.035 | 0.026 | 0.034 | 0.036 | 0.047 | 0.036 | 0.039 |
| K | 0.000 | 0.001 | 0.000 | 0.000 | 0.000 | 0.000 | 0.000 | 0.000 | 0.000 | 0.000 | 0.000 | 0.001 | 0.000 | 0.000 | 0.000 | 0.002 |
| Cr | 0.000 | 0.000 | 0.000 | 0.000 | 0.000 | 0.000 | 0.000 | 0.000 | 0.000 | 0.001 | 0.000 | 0.000 | 0.000 | 0.000 | 0.000 | 0.000 |
| Sum | 4.028 | 4.028 | 4.017 | 4.029 | 4.015 | 4.021 | 4.017 | 4.014 | 4.018 | 4.035 | 4.025 | 4.025 | 4.030 | 4.017 | 4.017 | 4.023 |
| Wo (mol %) | 43.8 | 44.9 | 43.5 | 45.5 | 46.3 | 45.8 | 44.6 | 45.8 | 45.7 | 46.1 | 47.3 | 43.9 | 44.8 | 44.7 | 44.5 | 43.3 |
| En | 44.0 | 43.7 | 44.4 | 42.7 | 42.0 | 42.5 | 43.3 | 42.7 | 43.1 | 42.4 | 41.5 | 43.7 | 43.7 | 43.2 | 43.3 | 44.5 |
| Fs | 12.1 | 11.4 | 12.1 | 11.9 | 11.7 | 11.7 | 12.0 | 11.5 | 11.3 | 11.5 | 11.2 | 12.3 | 11.5 | 12.0 | 12.2 | 12.2 |
| KD Fe/Mg, cpx/liq | 0.29 | 0.27 | 0.28 | 0.29 | 0.29 | 0.29 | 0.29 | 0.28 | 0.27 | 0.28 | 0.28 | 0.29 | 0.28 | 0.28 | 0.29 | 0.28 |
| [a]P(kbar) | 4.1 | 2.1 | 2.3 | 3.0 | 4.1 | 3.3 | 2.8 | 3.1 | 2.3 | 2.8 | 2.6 | 1.9 | 1.8 | 2.5 | 2.2 | 3.2 |
| [b]P(kbar) | 3.0 | 3.0 | 0.8 | 3.3 | 2.9 | 2.6 | 1.7 | 2.0 | 2.2 | 3.4 | 3.4 | 1.9 | 2.1 | 0.5 | 1.8 | 1.5 |

The whole rock compositions of the host lavas were used as representative of the melt, using only clinopyroxene-melt pairs as close as possible to the equilibrium value of 0.27±0.03 in geobarometric calculations

[a] Pressure derived according to Eq. 32a of Putirka (2008)

[b] Eq. 32c of Putirka (2008). The temperature for barometric calculations was fixed at 1,080 °C

**Table 4** Calculation of density (g/cm$^3$) and related $V_P$ (km/s) for the different groups of cognate xenoliths

| Group | Mineral | [a]Mineral density ($\rho_M$) (g/cm$^3$) | Average mineral abundance (vol %) | Average mineral weight ($W_M$) (wt %) | Calculated density ($\rho_C$) (g/cm$^3$) | Bulk density (g/cm$^3$) | [b]$V_P$ (km/s) |
|---|---|---|---|---|---|---|---|
| AMGB | Plg *(An80)* | 2.71 | 43 | 36 | 3.4 | 3.0 | 6.1 |
| | Cpx *($Wo_{45}$ $En_{42}$ $Fs_{13}$)* | 3.14 | 35 | 34 | | | |
| | Ol *(Fo76)* | 3.54 | 4 | 4 | | | |
| | Amph | 3.12 | 2 | 2 | | | |
| | Ti-mt *(Usp36)* | 4.95 | 16 | 24 | | | |
| AMMG | Plg *(An80)* | 2.71 | 23 | 20 | 3.2 | 2.8 | 5.6 |
| | Cpx *($Wo_{45}$ $En_{42}$ $Fs_{13}$)* | 3.14 | 21 | 21 | | | |
| | Ol *(Fo76)* | 3.54 | 2 | 2 | | | |
| | Amph | 3.12 | 49 | 49 | | | |
| | Ti-mt *(Usp36)* | 4.95 | 5 | 8 | | | |
| OLLG | Plg *(An85)* | 2.71 | 62 | 55 | 3.1 | 2.7 | 5.2 |
| | Cpx *($Wo_{46}$ $En_{40}$ $Fs_{14}$)* | 3.14 | 19 | 20 | | | |
| | Ol *(Fo71)* | 3.59 | 13 | 15 | | | |
| | Ti-mt *(Usp46)* | 4.90 | 6 | 10 | | | |
| AMLG | Plg *(An76)* | 2.70 | 69 | 62 | 3.1 | 2.7 | 5.2 |
| | Cpx *($Wo_{44}$ $En_{43}$ $Fs_{13}$)* | 3.14 | 17 | 18 | | | |
| | Ol *(Fo76)* | 2.54 | 4 | 5 | | | |
| | Amph | 3.12 | 3 | 33 | | | |
| | Ti-mt *(Usp39)* | 4.94 | 7 | 12 | | | |
| PLLG | Plg *(An54)* | 2.68 | 86 | 81 | 3.0 | 2.6 | 4.9 |
| | Bt *(XMg= 0.63)* | 2.94 | 7 | 7 | | | |
| | Ti-mt *(Usp42)* | 4.92 | 7 | 12 | | | |

E.g. for a plagioclase $An_{76}$ (end-members: albite $\rho$=2.62 g/cm$^3$; anorthite $\rho$=2.73 g/cm$^3$), the calculation is as follows: (76×2.73+24×2.62)/100= 2.70 g/cm$^3$. The same approach has been used to calculate the density of: i) olivine, (forsterite $\rho$=3.27 g/cm$^3$, fayalite $\rho$=4.39 g/cm$^3$); ii) clinopyroxene (wollastonite 2.84 g/cm$^3$, enstatite $\rho$=3.20 g/cm$^3$, ferrosilite $\rho$=3.95 g/cm$^3$); iii) Ti-magnetite (magnetite $\rho$=5.15 g/cm$^3$, ulvospinel $\rho$=4.60 g/cm$^3$) and biotite (phlogopite $\rho$=2.80 g/cm$^3$, annite $\rho$=3.17 g/cm$^3$). For amphibole, the density of Mg-hastingsite (3.12 g/cm$^3$) has been considered

See Section "Calculation of xenolith densities and derived P-wave velocity" for details

[a] For mineral solid solutions, density was calculated taking in account the density of end-members and the mean mineral composition for the given assemblage

[b] Following Gebrande et al. (1982), the calculated $V_P$ (km/s) value is ±0.18

that the cognate xenoliths might be fragments of the magmatic rocks forming the HVB, in a depth range confined between 3 and 13 km b.s.l.

## Discussion

To understand the origin of the cognate xenoliths, we firstly hypothesized if they could be "comagmatic", i.e., they might represent the slowly cooled counterparts of the respective host lavas. In principle, in the ideal case of equilibrium crystallization, the bulk composition of the cognate xenolith and host lavas should be similar. In reality, each cumulate is the result of a particular combination of properties (cotectic ratios, phase densities, etc.) and processes (melt expulsion due to filter-press, etc.) so that, very rarely, it has the composition of the former liquid. This latter could be the reason for the significant compositional difference among our xenoliths and their host lavas (Table 2 and Figs. 5, 6, 8). A "comagmatic" relationship is further weakened by the mineral chemistry of the cognate xenoliths, suggesting that there is a chemical disequilibrium between olivine in AMLG and OLLG and the melt (represented by the bulk rock compositions of 2001 and 2002–03 host lavas). Indeed, assuming a $KD_{Fe\text{-}Mg}^{oliv\text{-}liq}$=0.30 (Roeder and Emslie 1970), olivine in AMLG (mean core=$Fo_{76}$ in 2001-INCL) and OLLG (mean core=$Fo_{71}$ in 02NE05) should be in equilibrium with melts having Mg# (=100*Mg/Mg+$Fe_{tot}$) =0.49 and Mg#=0.42 respectively, i.e. melts Mg-poorer than 2001 and 2002–03 host lavas, whose Mg# is 0.52 (Table 2).

### The formation of the cognate xenolith hosted in 1763 lavas

Once the comagmatic nature of the studied xenoliths was ruled out, we then explored the possibility that a xenolith could derive from the crystal fractionation of a DDF magma that was stored in the deep portion (>5 km b.s.l.) of the Mt. Etna plumbing system, and is represented by the composition of the 1763 "La Montagnola" host rock. When a parent

**Table 5** Density measurements of samples XET and 2001-INCL performed with a hydrostatic balance (for details see Section "Sampling and analytical methods")

| Sample | XET | | | Sample | 2001-INCL | | |
|---|---|---|---|---|---|---|---|
| Fragment | Wa | Wl | ρs | Fragment | Wa | Wl | ρs |
| 1 | 4.23 | 2.63 | 2.64 | 1 | 5.15 | 3.17 | 2.60 |
| 2 | 7.16 | 4.44 | 2.63 | 2 | 3.94 | 2.43 | 2.61 |
| 3 | 10.09 | 6.14 | 2.55 | 3 | 4.49 | 2.77 | 2.62 |
| 4 | 7.24 | 4.43 | 2.57 | 4 | 8.80 | 5.46 | 2.63 |
| 1 bis | 4.25 | 2.62 | 2.60 | 1 bis | 5.19 | 3.20 | 2.61 |
| 2 bis | 7.21 | 4.43 | 2.60 | 2 bis | 3.97 | 2.46 | 2.63 |
| 3 bis | 10.14 | 6.17 | 2.55 | 3 bis | 4.52 | 2.80 | 2.62 |
| 4 bis | 7.33 | 4.49 | 2.58 | 4 bis | 8.88 | 5.52 | 2.65 |
| average | | | **2.59** | average | | | **2.62** |
| 1σ | | | **0.03** | 1σ | | | **0.01** |

A sample was broken into four fragments and each one was measured twice (i.e., fragment "1" and "1 bis"). *Wa* weight of a fragment in air, *Wl* weight of a fragment in water; $\rho_S$ measured density of the fragment

magma crystallizes different minerals, the residual liquid follows a path defined as the liquid line of descent (LLD) and, for porphyritic rocks (Cox et al. 1979), it can be graphically drawn by a tie-line linking the bulk composition of the parent rock to groundmass. Following this criterion, the LLDs of 1763, 2001 and 2002–03 parental magmas have been drawn in a CaO vs. MgO diagram (dashed lines in Fig. 8) by connecting the bulk rock with the respective groundmass glass (for References, see Fig. 8 caption).

Only the 1763-INCL xenolith plots very close to the LLD of its host lava (Fig. 8). Moreover, since the 1763-INCL is much

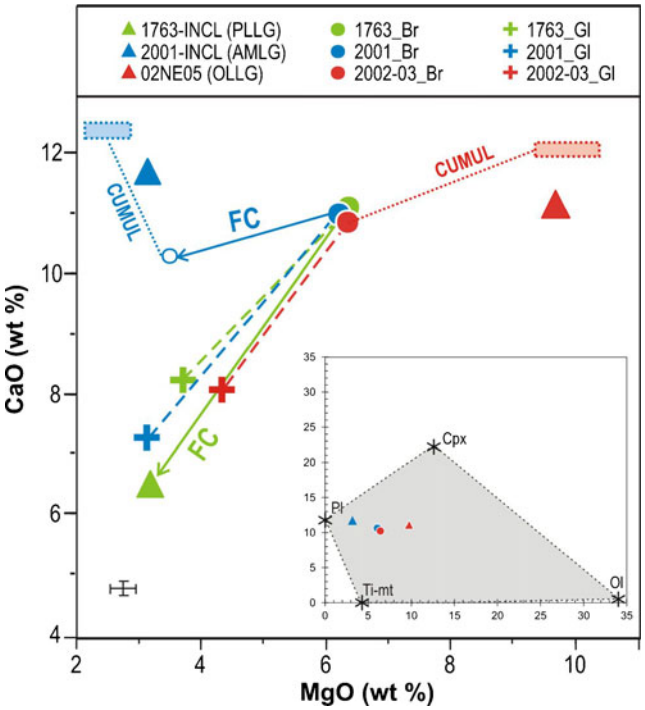


**Fig. 8** CaO vs. MgO diagram for bulk rock compositions of cognate xenoliths (1763-INCL, 2001-INCL, 02NE05) and the average of the 1763, 2001 and 2002–03 host lavas (data are respectively from: Corsaro et al. 2009b; Corsaro et al. 2007; Corsaro et al. 2009a). In the legend, "Br" is for "Bulk rock". Residual glass of host lavas (1763_Gl, 2001_Gl, 2002-03_Gl) are plotted (Miraglia 2002 for 1763 products; Corsaro et al. 2007 for 2001; Miraglia personal communication for 2002–03). *Dashed lines* describe the liquid line of descent (LLD) connecting a parental magmas to the correspondent groundmass glass composition. For the explanation of the FC arrow, dotted line CUMUL and rectangular areas, see Fig. 6. The bulk composition of the xenoliths 2001-INCL and 02NE05 (inset) lie within the polygon whose apexes are defined by the average composition of crystallizing mineral phases

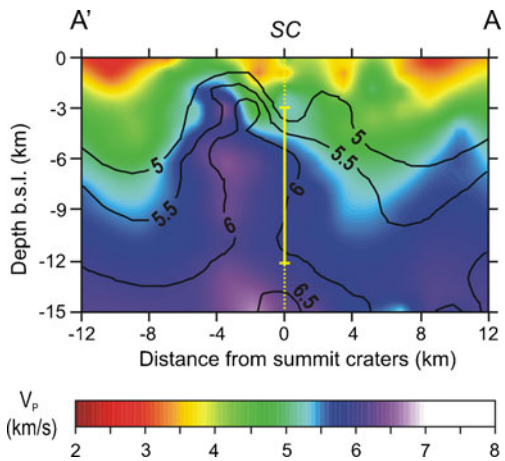


**Fig. 7** N-S vertical section crossing the summit craters derived from Patanè et al. (2006) 3D-velocity model (see Figs. 1 and 2 to locate the profile). The black lines are isovelocity contours in the range 5–6.5 km/s, at 0.5-km/sec intervals. The vertical yellow solid line indicates the depth range (3–12 km b.s.l.) encompassing the $V_P$ calculated following Gebrande (1982)

richer (Fig. 5) in $SiO_2$ (=51.41 %) and alkali (=6.95 %) than the 1763 lavas ($SiO_2$=47.27 % and alkali=4.73 %), it could be a residual liquid of the parental magma represented the by 1763 host rock. We then modeled a fractional crystallization (FC) (Stormer and Nicholls 1978) that started from the 1763 "La Montagnola" host lava and generated a melt with the composition of the 1763-INCL xenolith. The removal of 23 wt.% Cpx, 14 wt.% Plg, 4 wt.% Ti-mt, 3 wt.% Bt and 2 wt.% Ol, having the compositions of the minerals measured in the 1763 lavas (Miraglia 2002: average values Plg = $An_{80}$, Ol = $Fo_{73}$, Cpx = $Wo_{47}En_{39}Fs_{14}$ and Ti-mt = $Usp_{37}$), and in the sample 1763-INCL (average Bt with Mg/Mg + Fetot = 0.64), provides a good fit ($R^2$ = sum of square residuals = 0.2) between the measured and modeled compositions of the 1763-INCL xenolith (see the green arrow of FC pattern in Fig. 8).

We further tested the FC process by trace elements modeling with the Rayleigh's equation, using the previously calculated percentages of fractionating minerals and the partition coefficients (D) of D'Orazio et al. (1998) for Mt. Etna

products. We excluded biotite from the calculation due to the difficulty to assign a reliable D for an alkali basaltic melt. The error between modeled and measured trace elements content is fairly good (< 15 %) for most trace elements (see green arrows of FC patterns in Fig. 6), with the exception of Cr and Ni (>25 %). Overall, both major and trace element models support the hypothesis that the 1763-INCL xenolith represents a liquid that differentiated from a DDF parental magma with the composition of the 1763 host lava, due to the subtraction of 46 % mineral phases consisting of clinopyroxene, plagioclase, Ti-magnetite, biotite and olivine.

FC mass balance calculations were also performed starting from parental DDF magmas with the composition of the 2001 and 2002–03 host lavas (Table 3) to verify if, respectively, the 2001-INCL and 02NE05 cognate xenoliths could represent residual liquids. Fractionating minerals were from Corsaro et al. (2007): Plg = $An_{83}$, Ol = $Fo_{79}$, Cpx = $Wo_{49}En_{37}Fs_{14}$ and Ti-mt = $Usp_{47}$. Nonetheless, the results of the modeling are unsatisfactory, since $R^2$ is respectively=2.1 and 1.9. The fact that the process of "subtraction" of crystals from the 2001 and 2002–03 parental magma is inconsistent in explaining the composition of 2001-INCL and 02NE05 cognate xenoliths is furthermore evidenced in Fig. 8, where both are entirely outside the respective LLDs.

## The formation of the cognate xenolith hosted in the 2001 and 2002–03 lavas

Crystal-melt fractionation mechanisms in a magmatic plumbing system may be very complex, and we therefore investigated the origin of the 2001-INCL and 02NE05 cognate xenoliths by formulating the hypothesis that minerals are "added" to the DDF magma stored in a deep region of the volcano plumbing system, and not "subtracted", as suggested in the Section "The formation of the cognate xenolith hosted in 1763 lavas". In this view, the 2001 and 2002–03 DDF magmas, represented by the composition of the 2001 and 2002–03 host lavas (Table 3), should have experienced enrichment of crystals to produce rocks with the composition of the 2001-INCL and O2NE05 cognate xenoliths, respectively. This hypothesis is supported by petrographic data that mostly show the abundance of plagioclase, with a modal ratio of Plg/Cpx=3.5 for AMLG (2001-INCL) and 2.8 for OLLG (02NE05). These values are well above the range of other cognate xenoliths (Plg/Cpx=0.9–1.1, Table 1) and the experimental cotectic ratio of high-K basalts (0.30–0.45, for pressure in the range 1–4 kbar; Di Carlo et al. 2006). Therefore, we modeled a crystal accumulation process by a linear mixing calculation, which is

**Table 6** Mixing calculation for major and selected trace elements to model the composition of a cumulitic rock (Z) formed for the accumulation of a crystals assemblage (X) to a melt (Y). For details see the text. Y= bulk rock composition of 2002-03 host lava; X= Plg, Cpx, Ol and Ti-mt compositions are average of measurements performed in 02NE05 cognate xenolith; Z= the composition of cumulitic rock is provided as a range confined by the values of the fraction of minerals accumulated (N)

| | Melt (Y) | Cumulus crystals (X) | | | | Cumulate (Z) | | |
|---|---|---|---|---|---|---|---|---|
| Fraction accumulated (N) | 2002–03 Host lava | Plg $An_{85}$ 0.40–0.45 | Cpx $Wo_{46}En_{40}Fs_{14}$ 0.09–0.11 | Ol $Fo_{71}$ 0.16–0.20 | Ti-mt $Usp_{46}$ 0.05–0.06 | | 02NEO5 | [a]Error % |
| $SiO_2$ | 47.31 | 46.75 | 48.93 | 37.35 | 0.12 | 42.41–43.28 | 44.55 | 3–5 |
| $TiO_2$ | 1.67 | 0.03 | 1.52 | 0.03 | 14.45 | 1.35–1.37 | 1.18 | 15–17 |
| $Al_2O_3$ | 16.71 | 34.39 | 5.51 | 0.04 | 5.52 | 19.43–19.54 | 17.85 | 9–10 |
| FeO | 10.31 | 0.44 | 8.20 | 25.29 | 68.79 | 11.49–12.14 | 11.72 | 2–4 |
| MnO | 0.17 | 0.01 | 0.20 | 0.55 | 0.46 | 0.18–0.19 | 0.18 | 2–8 |
| MgO | 6.36 | 0.04 | 13.58 | 36.09 | 4.52 | 9.15–10.14 | 9.76 | 4–6 |
| CaO | 10.91 | 17.03 | 21.56 | 0.35 | 0.00 | 12.07–12.08 | 11.11 | 8 |
| Alkali | 5.23 | 1.67 | 0.58 | 0.02 | 0.02 | 1.76–2.29 | 2.67 | 14–34 |
| Co | 41.2 | 0.1 | 41 | 190 | 225 | 57.7–63.5 | 66.4 | 4–13 |
| V | 299 | 1 | 324 | 15 | 2797 | 261–262 | 297 | 11–12 |
| Ba | 560 | 130 | 0.05 | 27.4 | 2.15 | 165–224 | 268 | 15–38 |
| Sr | 1063 | 2132 | 122 | 32 | 2.67 | 1193–1208 | 1276 | 5–6 |
| Th | 6.89 | 0.01 | 0.06 | 0.71 | 0.08 | 1.40–2.19 | 1.58 | 12–38 |
| Yb | 2.11 | 0.02 | 0.98 | 0.24 | 0.05 | 0.55–0.77 | 0.70 | 9–22 |

[a] The error is the difference between the composition of the modeled cumulate (Z) and the composition of the xenolith, divided for the composition of the xenolith and expressed as percentage

simply the numerical expression of the lever rule (Cox et al. 1979; Ragland 1989). The composition of the cumulus crystals (X), the melt (Y), the cumulate (Z) and the fraction of crystals accumulated (N) are linearly related by the equation (Eq. 5.23 in Ragland 1989):

$$Z = NX + (1-N)Y$$

To model the composition of 02NE05 cognate xenoliths embedded in the 2002–03 lavas, the following variables were included in the above equation (Table 6): $Y$ = average bulk rock composition of 2002–03 host lava, and $X$ = composition of the cumulus assemblage, made of the minerals forming the 02NE05 xenolith, i.e., Plg, Cpx, Ol and Ti-mt. The major element composition of minerals is the average of the EMPA measurements performed on the 02NE05 xenolith (Table 6, Plg = $An_{85}$, Cpx = $Wo_{46}En_{40}Fs_{14}$, Ol = $Fo_{71}$ and Ti-mt = $Usp_{46}$). The trace element contents of minerals (Table 6) are derived from the literature, by choosing the minerals with compositions as close as possible to those of the 02NE05 cognate xenolith. In particular, the trace elements of Plg and Cpx are from Viccaro et al. (2006), and Ol and Ti-mt are from D'Orazio et al (1998). The NX term of the equation above is then calculated as: $NX = X_{Pl} \times N_{Pl} + X_{Ol} \times N_{Ol} + X_{Cpx} \times N_{Cpx} + X_{Ti\text{-}mt} \times N_{Ti\text{-}mt}$. We set a range for N, i.e., the fraction of crystals accumulated, and solved the equation above for Z (Table 6). Calculations have been carried out separately for all major and selected trace elements (Co, V, Ba, Sr, Th, Yb). The discrepancy between the composition of the modeled cumulate (Z) and the 02NEO5 xenolith has been expressed as error (%) (Table 6). The results indicate that, by adding 40–45 % Plg, 16–20 % Ol, 9–11 % Cpx, and 5–6 % Ti-mt to the 2002–03 DDF magma, there is a fairly good match between the modeled cumulate and the 02NE05 xenolith. In fact, the low limit of the errors (Table 6), remains ≤15 % for both major and trace elements. These values may be considered acceptable, taking into account the uncertainty of laboratory measurements (see Section "Sampling and analytical methods") and a further source of inaccuracy for the use of trace element compositions not directly measured in the studied samples. The reliability of the results obtained is also evident in Figs. 6 and 8 where, respectively for trace and major elements, it can be viewed that the compositional range of the modeled cumulate (red-colored rectangle) overlaps, or is close, to the composition of the 02NE05 xenolith.

Following the above approach, we finally tried to model the composition of the 2001-INCL contained in the 2001 lavas. Nevertheless, to account for the major element composition and for the very low content of some compatible elements in the 2001-INCL (i.e., Cr=5.6 ppm and Ni=8.0 ppm),

**Table 7** Mixing calculation for major and selected trace elements to model the composition of a cumulitic rock (Z) formed for the accumulation of a crystals assemblage (X) to a melt (Y). For details see the text. Y= composition of a melt fractionated from 2001 host lavas for the subtraction of 10% Cpx and 5% Ol; X= Plg, Cpx, Ol and Ti-mt compositions are average of measurements performed in 2001-INCL. Z= the composition of cumulitic rock is provided as a range confined by the values of the fraction of minerals accumulated (N)

| | Melt (Y) | Cumulus crystals (X) | | | | Cumulate (Z) | | |
|---|---|---|---|---|---|---|---|---|
| Fraction accumulated (N) | [a]2001 fractionated Host lava | Plg $An_{76}$ 0.45–0.50 | Cpx $Wo_{44}En_{43}Fs_{13}$ 0.02–0.03 | Ol $Fo_{71}$ 0.00–0.02 | Ti-mt $Usp_{39}$ 0.02–0.03 | | 2001-INCL | [b] Error % |
| $SiO_2$ | 48.17 | 48.79 | 51.52 | 38.50 | 0.08 | 46.95–47.56 | 47.64 | 0–1 |
| $TiO_2$ | 1.83 | 0.07 | 0.96 | 0.05 | 13.15 | 1.23–1.25 | 1.34 | 7–8 |
| $Al_2O_3$ | 19.25 | 32.94 | 3.11 | 0.05 | 4.61 | 24.79–24.81 | 22.27 | 11 |
| FeO | 10.10 | 0.29 | 7.22 | 22.02 | 71.53 | 6.85–7.19 | 8.29 | 13–17 |
| MnO | 0.15 | 0.02 | 0.34 | 0.74 | 0.64 | 0.11–0.12 | 0.13 | 8–17 |
| MgO | 3.48 | 0.02 | 15.16 | 39.25 | 4.45 | 2.18–2.85 | 3.18 | 10–30 |
| CaO | 10.26 | 15.20 | 21.52 | 0.22 | 0.00 | 12.50–12.56 | 11.73 | 1–7 |
| Alkali | 6.19 | 2.68 | 0.54 | 0.02 | 0.03 | 3.96–4.38 | 4.33 | 8 |
| Co | 30.0 | 0.2 | 42 | 175 | 198 | 20.2–23.4 | 25.0 | 7–20 |
| V | 306 | 1 | 277 | 13 | 3168 | 225–233 | 202 | 11–15 |
| Ba | 664 | 117 | 0.064 | 27.3 | 10.8 | 338–391 | 455 | 13–26 |
| Sr | 1262 | 2711 | 137 | 50 | 45 | 1867–1892 | 2179 | 13–14 |
| Th | 8.87 | 0.02 | 0.12 | 0.69 | 0.88 | 3.78–4.55 | 3.81 | 1–19 |
| Yb | 2.19 | 0.01 | 1.86 | 0.37 | 0.38 | 1.00–1.17 | 1.14 | 2–12 |

[a] Melt formed for the fractionation of 10% Cpx and 5% Ol starting from the 2001 host lava

[b] The error is the difference between the composition of the modeled cumulate (Z) and the composition of the xenolith, divided for the composition of the xenolith and expressed as percentage

we had to assume that the melt (Y) did not have the same composition as the 2001 host lavas, but rather that of a liquid slightly evolved from the 2001 host lavas for the subtraction of 10 % Cpx ($Wo_{49}En_{37}Fs_{14}$) and 5 % Ol ($Fo=_{79}$) (see Table 7 and open blue circle in Figs. 6 and 8). Therefore, the values inserted in the equation above were (Table 7): $Y$ = composition of the melt fractionated from 2001 host lavas, $X$ = composition of the cumulus assemblage formed by the minerals (Plg, Cpx, Ol and Ti-mt) present in the 2001-INCL xenolith. The major element composition of each mineral is the average of EMPA measurements of the 2001-INCL xenolith (Plg = $An_{76}$, Cpx = $Wo_{44}En_{43}Fs_{13}$, Ol = $Fo_{71}$, Ti-mt=$Usp_{39}$). The trace element composition is derived from literature data selected from Viccaro et al. (2006) for Plg and Cpx and from D'Orazio et al. (1998) for Ol and Ti-mt.

The modeling (Table 7 and Figs. 6 and 8) suggests that the addition of 45–50 % Plg, 2–3 % Cpx, 2–3 % Ti-mt and 0–2 % Ol to a melt slightly more evolved than 2001 host lavas accounts for the composition of the 2001-INCL xenolith. The error is ≤13 % for both major and trace elements, and thus is comparable with the ones calculated for the modeling of the 02NE05 xenolith.

### Origin of the cognate xenoliths at the "solidification front"

The reconstruction of an intrusive setting for the formation of the rocks that generated the studied cognate xenoliths is a demanding task, on which we speculate below.

Petrologic and geophysical studies performed over recent decades suggest that Mt. Etna's plumbing system is rather complex and consists of different reservoirs, both inside the volcanic edifice and the substratum (for an overview, see Bonaccorso et al. 2004). For our purposes, we stress the role played by a deeper zone (>5 km b.s.l., Spilliaert et al. 2006) of the magmatic plumbing system, where deep dyke-fed (DDF) basaltic magmas are stored and maintain a fairly stable composition over time, as indicated by the homogeneity of the 1763, 2001 and 2002–03 lavas emitted during DDF eruptions. We suggest that most of the studied cognate xenoliths originated from gabbroic intrusive rocks that formed at the "solidification front" (SF, Marsh 1996, 2000), i.e., a marginal zone of Mt. Etna's deep plumbing system, within which crystallization of DDF magmas took place. The structure of this zone is quite complex in terms of rheological properties of the magma (Marsh 1996, 2000) and, on the whole, a chemical differentiation of the resident DDF magma may occur for the physical separation of the crystallizing minerals and the melt.

In particular, the cognate xenolith hosted in the 1763 lavas has been interpreted (see Section "The formation of the cognate xenolith hosted in 1763 lavas") as a residual melt that differentiated from a DDF 1763 magma for the fractionation of 46 % minerals. This process probably began in an inner zone of the solidification front, where the viscosity of the system was low and the crystallizing minerals were free to escape from the melt and fractionate. When the content of minerals progressively increased, the formation of a crystalline mesh made the solid–liquid separation less efficient. In these conditions, we argue that most likely the load of minerals and/or an instability induced by a refilling event may have caused the breakage of the crystal mesh and filter-pressing of the residual melt, which cooled and crystallized in separate vein/lens, forming an intrusive rock represented by the 1763-INCL xenolith.

In the same environment, the breakage of the crystalline mesh may have also caused the detachment of clumps/clusters of minerals. They may be sunk and accumulated in a still-hot zone of the solidification zone, where the original DDF magma was resident. With this mechanism, the accumulation of 40–45 % Plg, 16–20 % Ol, 9–11 % Cpx and 5–6 % Ti-mt in a 2002–03 DDF magma explains the formation of intrusive rocks that generated a OLLG-type xenolith (02NE05) (see Section "The formation of the cognate xenolith hosted in 2001 and 2002–03 lavas"). In the same way, the addition of 45–50 % Plg, 2–3 % Cpx, 2–3 % Ti-mt and 0–2 % Ol to a slightly evolved 2001 DDF magma justifies the formation of an AMLG–type xenolith (2001-INCL) (see Section "The formation of the cognate xenolith hosted in 2001 and 2002–03 lavas").

Looser constraints can be set for the formation of the other two amphibole-bearing cognate xenoliths (AMGB, AMMG), largely due to the lack of whole-rock analyses. Their mineral chemistry is similar to the cognate xenoliths hosted in the 2001 lavas (Clocchiatti et al. 2004; Corsaro et al. 2007; Viccaro et al. 2007), for which a crystallization at $P_{H2O}$>0.75 kbar has been suggested by the authors.

## Conclusions

The study of Mt. Etna's cognate xenoliths offered the opportunity to investigate an otherwise inaccessible environment, i.e., the roots of an active volcano, and to provide insights into the mineralogy and composition of the rocks forming its basement, as well as the processes taking place in the magmatic plumbing system.

The textural, mineralogical, compositional and physical properties of the cognate xenoliths hosted in the 1763 "La Montagnola", and the 2001 and 2002–03 lavas erupted by Mt. Etna, integrated with data derived from seismic inversions, rule out a mantle origin for xenoliths and shed light on the features of the high-velocity body (HVB) located S-SE of the summit craters up to a depth of 15 km b.s.l. (Chiarabba et al. 2004 and Patanè et al. 2006), hitherto exclusively imaged by seismic tomographies.

This anomalous high $V_P$ region, from 3 to 13 km b.s.l., consists of intrusive gabbroic rocks that chiefly developed at

the "solidification front".This front borders a deep region (> 5 km b.s.l.) of Mt. Etna's plumbing system where complex mechanisms of crystal-melt separation took place. The cognate xenoliths are fragments of the intrusive rocks that were transported to the surface by the volatile-rich and fast-ascending, deep dyke-fed (DDF) eruptions of 1763 ("La Montagnola"), 2001, and 2002–03.

Since seismological data (Patané et al. 2003; Cocina, unpublished data) show that the HVB is aseismic, it's reasonable to think that the solidified intrusive rocks are not actively involved in magma dynamics and represent a peripheral zone of the present-day plumbing system.

Although the "picture" of the HVB derived by the study of the cognate xenoliths is necessarily incomplete, due essentially to the small set of samples, this is the first attempt to characterize the mineralogical, compositional and physical properties of this anomalous $V_P$ region beneath Mt. Etna. Broadly speaking, our study demonstrates that the integration of petro-chemical and physical parameters of a rock, combined with seismic information, might prove a useful tool for investigating the roots of an active volcano plumbing system.

**Acknowledgments** This study was initiated thanks to G. Amendolia, geologist and volcanological guide, who collected many of the samples. We are also greatly indebted to V. Scribano for fruitful discussion and for having provided the sample XET. M. Viccaro and an anonymous reviewer greatly improved the clarity of this paper with helpful and thoughtful suggestions. We also wish to thank M.A. Clynne and two anonymous reviewers for their helpful comments on an early version of this manuscript. We are grateful to Graziella Barberi for the elaboration of the tomograms and to A. Cavallo for the assistance during EMPA measurements. Lucia Messina is thanked for rock powder preparations.

## References

Allard P, Behncke B, D'Amico S, Neri M, Gambino S (2006) Mount Etna 1993–2005: anatomy of an evolving eruptive cycle. Earth Sci Rev 78:85–114. doi:10.1016/j.earscirev.2006.04.002

Alletti M, Pompilio M, Rotolo SG (2005) Mafic and ultramafic enclaves from Ustica Island lava: inferences on deep magmatic processes. Lithos 84:151–167. doi:10.1016/j.lithos.2005.03.015

Aloisi M, Cocina O, Neri G, Orecchio B, Privitera E (2002) Seismic tomography of the crust underneath the Etna volcano, Sicily. Phys Earth Planet Inter 134:139–155. doi:10.1016/S0031-9201(02)00153-X

Aloisi M, Mattia M, Monaco C, Pulvirenti F (2011) Magma, faults and gravitational loading at Mt. Etna: the 2002–2003 eruptive period. J Geopyhs Res. doi:10.1029/2010JB007909, in press

Andronico D, Branca S, Calvari S, Burton MR, Caltabiano T, Corsaro RA, Del Carlo P, Garfì G, Lodato L, Miraglia L, Muré F, Neri M, Pecora E, Pompilio M, Salerno G, Spampinato L (2005) A multi-disciplinary study of the 2002–03 Etna eruption: insights into a complex plumbing system. Bull Volcanol 67:314–330. doi:10.1007/s00445-004-0372-8

Armienti P, Innocenti F, Petrini R, Pompilio M, Villari L (1988) Sub-aphyric alkali basalt from Mt. Etna: inferences on the depth and composition of the source magma. Rend Soc Ital Mineral Petrol 43:877–891

Aurisicchio C, Scribano V (1987) Some ultramafic xenoliths from Etna. Rend Soc Ital Mineral Petrol 42:219–224

Barberi G, Cocina O, Maiolino V, Musumeci C, Privitera E (2004) Insight into Mt. Etna (Italy) kinematics during the 2002–2003 eruption as inferred by seismic stress and strain tensors. Geophys Res Lett 31, L21614

Barclay J, Carmichael ISE (2004) A hornblende basalt from western Mexico: water saturated phase relations constrain a pressure-temperature window of eruptibility. J Petrol 45:485–506. doi:10.1093/petrology/egg091

Benz HM, Chouet BA, Dawson PB, Lahr JC, Page RA, Hole JA (1996) Three-dimensional P and S wave velocity structure of Redoubt Volcano, Alaska. J Geophys Res 101:8111–8128. doi:10.1029/95JB03046

Bonaccorso A et al (eds) (2004) Mt. Etna: volcano laboratory, geophysical monograph series, vol. 143. AGU, Washington, D. C

Bottari A, Lo Giudice E, Patané G, Romano R, Sturiale C (1975) L'eruzione etnea del Gennaio-Marzo 1974. Riv Miner Sic 154–156:175–199

Cardaci C, Coviello M, Lombardo G, Patané G, Scarpa R (1993) Seismic tomography of Etna volcano. J Volcanol Geotherm Res 56:357–368. doi:10.1016/0377-0273(93)90002-9

Chiarabba C, Amato A, Boschi E, Barberi F (2000) Recent seismicity and tomographic modeling at Mount Etna plumbing system. J Geophys Res 105:10923–10938. doi:10.1029/1999JB900427

Chiarabba C, De Gori P, Patanè D (2004) The Mt. Etna Plumbing System: the Contribution of Seismic Tomography. In: Bonaccorso A, Calvari S, Coltelli M, Del Negro C, Falsaperla S (eds) Etna volcano laboratory. Gephys Monogr AGU 143:191–204

Clocchiatti R, Condomines M, Guénot N, Tanguy JC (2004) Magma changes at Mount Etna: the 2001 and 2002–2003 eruptions. Earth Planet Sci Lett 226:397–414. doi:10.1016/j.epsl.2004.07.039

Corazzato C, Francalanci L, Menna M, Petrone C, Renzulli A, Tibaldi A, Vezzoli L (2008) What controls sheet intrusion in volcanoes? Petrological and structural characters of the Stromboli sheet complex, Italy. J Volcanol Geotherm Res 173:26–54. doi:10.1016/j.jvolgeores.2008.01.006

Corsaro RA, Pompilio M (2004a) Magma dynamics in the shallow plumbing system of Mt.Etna as recorded by compositional variations in volcanics of recent summit activity (1995–1999). J Volcanol Geotherm Res 137(1–3):55–71

Corsaro RA, Pompilio M (2004b) Buoyancy-controlled eruptions of magmas at Mt. Etna Terra Nova 16:6–22. doi:10.1046/j.1365-3121.2003.00520.x

Corsaro RA, Miraglia L, Pompilio M (2007) Petrologic evidence of a complex plumbing system feeding the July-August 2001 eruption of Mt Etna, Sicily, Italy. Bull Volcanol 69:401–421. doi:10.1007/s00445-006-0083-4

Corsaro RA, Civetta L, Di Renzo V, Miraglia L (2009a) Petrology of lavas from 2004–05 eruption of Mt. Etna, Italy: inferences on the dynamics of magma in the central conduits plumbing system. Bull. Volcanol 71(7):781–793. doi:10.1007/s00445-009-0264-z

Corsaro RA, Métrich N, Allard P, Andronico D, Miraglia L, Fourmentraux C (2009b) The 1974 flank eruption of Mount Etna: an archetype for deep dike-fed eruptions at basaltic volcanoes and a milestone in Etna's recent history. J Geophys Res 114, B07204. doi:10.1029/2008JB006013

Cox KG, Bell JD, Pankhurst RJ (1979) The interpretation of igneous rocks. George Allen and Unwin Publisher, 464 pp

D'Orazio M, Armienti P, Cerretini S (1998) Phenocryst/matrix trace-element partition coefficients for hawaiite-trachyte lavas from the Ellittico volcanic sequence (Mt. Etna, Sicily, Italy). Miner Petrol 64:65–88

De Luca G, Filippi L, Patanè G, Scarpa R, Vinciguerra S (1997) Three-dimensional velocity structure and seismicity of Mount Etna

volcano, Italy. J Volcanol Geotherm Res 79:123–138. doi:10.1016/S0377-0273(97)00026-7

Di Carlo I, Pichavant M, Rotolo SG, Scaillet B (2006) Experimental crystallization of a high-K arc basalt: the golden pumice, Stromboli volcano (Italy). J Petrol 47(7):1317–1343. doi:10.1093/petrology/egl011

Ferlito C, Viccaro M, Nicotra E, Cristofolini R (2012) Regimes of magma recharge and their control on the eruptive behaviour during the 2001–2005 period at Mt. Etna (Italy). Bull Volcanol 74:533–543

Gebrande H, Kern H, Rummel F (1982) Elasticity and inelasticity. In: Hellwege KH (ed) Landolt-Bornstein numerical data and functional relationship in science and technology. New series, group V: Geophys Space Res, vol. 1, physical properties of rocks, subvolume b. Springer, Berlin, pp 1–233

Grapes RH, Wysoczanski RJ, Hoskin PW (2003) Rhonite paragenesis in pyroxenite xenoliths, Mont Sidley volcano, Marie Byrd Land, West Antarctica. Mineral Mag 67(4):639–651. doi:10.1180/0026461036740123

Hirn A, Nercessian A, Sapin M, Ferrucci F, Wittlinger G (1991) Seismic heterogeneity of Mt. Etna: structure and activity. Geophys J Int 105:139–153. doi:10.1111/j.1365-246X.1991.tb03450.x

Holness MB, Anderson AT, Martin V, Maclennan J, Passmore E, Schwindinger K (2007) Textures in partially solidified crystalline nodules: a window into the pore structure of slowly cooled mafic intrusions. J Petrol 48(7):1243–1264. doi:10.1093/petrology/egm016

Huckenholz HG, Kunzmann T, Spicker C (1988) Stability of titanian magnesio-hastingsite and its breakdown to rhönite-bearing assemblages. Terra Cognita 8:66

Iezzi G, Mollo S, Ventura G, Cavallo A, Romano C (2008) Experimental solidification of anhydrous latitic and trachytic melts at different cooling rates: the role of nucleation kinetics. Chem Geol 253:91–101

Kozlovskaya E, Elo S, Hjelt SE, Yliniemi J, Pirttijarvi M, SVEKALAPKO Seismic Tomography Working Group (2004) 3-D density model of the crust of southern and central Finland obtained from joint interpretation of the SVEKALAPKO crustal *P*-waves velocity models and gravity data. Geophys J Int 158:827–848. doi:10.1111/j.1365-246X.2004.02363.x

Kunzmann T (1989) Rhönit: mineralchemie, paragenese und stabilitat in alkalibasaltischen vulkaniten. Ein beitrag zur minerogenese der Rhönit-anigmatit-mischkristallgruppe. PhD dissertation, Ludvig-Maximillians University, Munich

Laigle M, Hirn A (1999) Explosion-seismic tomography of a magmatic body beneath Etna: volatile discharge and tectonic control of volcanism. Geophys Res Lett 26(17):2665–2668. doi:10.1029/1998GL005300

Laigle M, Hirn A, Sapin M, Lepine JC, Diaz J, Gallart J, Nicolich R (2000) Mount Etna dense array local earthquake P and S tomography and implications for volcanic plumbing. J Geophys Res 105(B9):21623–21646. doi:10.1029/2000JB900190

Laiolo M, Cigolini C (2006) Mafic and ultramafic xenoliths in San Bartolo lava field: new insights on the ascent and storage of Stromboli magmas. Bull Volcanol 68:653–670

Le Maitre RW (ed) (2002) A classification of igneous rocks and glossary of terms. Recommendations of the IUGS subcommission on the systematics of the igneous rocks. Cambridge University Press

Leake BE, Woolley AR, Arps CES, Birch WD, Gilbert MC, Grice JD, Hawthorne FC, Kato A, Kisch HJ, Krivovichev VG, Linthout K, Laird J, Mandarino JA, Maresch WV, Nickel EH, Rock NMS, Schumacher JC, Smith DC, Stephenson NCN, Ungaretti L, Whittaker EJW, Youzhi G (1997) Nomenclature of amphiboles: report of the subcommittee on amphiboles of the international mineralogical association, commission on new minerals and mineral names. Am Mineral 82:1019–1037

Lees JM (1992) The magma system of Mount St. Helens: non linear high-resolution P-wave tomography. J Volcanol Geotherm Res 53:103–116. doi:10.1016/0377-0273(92)90077-Q

Lo Giudice A, Ritmann L (1975) Su alcune accumuliti etnee: aspetti mineralogici e genetici. Riv Mineraria Sicil 26:1–12

Marsh BD (1996) Solidification fronts and magmatic evolution. Mineral Mag 60:5–40

Marsh BD (2000) Magma chambers. In: Sigurdsson et al. (eds) Encyclopedia of volcanoes. Academic Press, pp 191–206

Mattioli M, Serri G, Salvioli-Mariani E, Renzulli A, Holm PM, Santi P, Venturelli G (2003) Sub-volcanic infiltration and syn-eruptive quenching of liquids in cumulate wall-rocks: the example of the gabbroic nodules of Stromboli (Aeolian Islands, Italy). Miner Petrol 78:201–230. doi:10.1007/s00710-002-0232-1

Métrich N, Allard P, Spilliaert N, Andronico D, Burton M (2004) 2001 flank eruption of the alkali and volatile-rich primitive basalt responsible for Mount Etna's evolution in the last three decades. Earth Planet Sci Lett 228:1–17. doi:10.1016/j.epsl.2004.09.036

Miraglia L (2002) Evidence for heterogeneous magmas in the feeding system of the 1763 "La Montagnola" eruption at Mount Etna. Plinius 27:108–112

Nicotra E, Viccaro M (2012) Unusual magma storage conditions at Mt. Etna (Southern Italy) as evidenced by the emission of plagioclase megacryst-bearing lavas: implications for the volcano plumbing system. Bull Volcanol 74:795–815

Okubo PG, Benz HM, Chouet BA (1997) Imaging the crustal magma sources beneath Mauna Loa and Kilauea volcanoes, Hawaii. Geology 25:867–870. doi:10.1130/0091-7613(1997)025<0867:ITCMSB>2.3.CO;2

Patanè D, Chiarabba C, Cocina O, De Gori P, Moretti M, Boschi E (2002) Tomographic images and 3D earthquake locations of the seismic swarm preceding the 2001 Mt. Etna eruption: evidence for a dyke intrusion. Geophys Res Lett 29:10

Patané D, De Gori P, Chiarabba C, Bonaccorso A (2003) Magma ascent and the pressurization of Mount Etna's volcanic system. Science 299:2061–2063. doi:10.1126/science.1080653

Patanè D, Barberi G, Cocina O, De Gori P, Chiarabba C (2006) Time-resolved seismic tomography detects magma intrusions at Mount Etna. Science 313:821–823. doi:10.1126/science.1127724

Pompilio M, Rutherford MJ (2002) Pre-eruption conditions and magma dynamics of recent amphiboles-bearing Etna basalt. Eos Trans AGU 82(47):F1412

Putirka K (2008) Thermometers and barometers for volcanic systems. Rev Mineral Geochem 69:61–120

Ragland PC (1989) Basic analytical petrology. Oxford Univ Press, New York, 369 p

Renzulli A, Santi P (1997) Sub-volcanic crystallization at Stromboli (Aeolian Islands, Southern Italy) preceding the Sciara del Fuoco sector collapse: evidence from monzonite lithic-suite. Bull Volcanol 59:10–20

Rittmann A (1965) Notizie sull'Etna. Supplemento al Nuovo Cimento 3(I):1117–1123

Roeder PL, Emslie RF (1970) Olivine-liquid equilibrium. Contrib Mineral Petrol 29:275–289. doi:10.2138/am.2005.1449

Rollin PJ, Cassidy J, Locke CA, Rymer H (2000) Evolution of the magmatic plumbing system at Mt Etna: new evidence from gravity and magnetic data. Terra Nova 12:193–198. doi:10.1046/j.1365-3121.2000.00285.x

Schiavone D, Loddo M (2007) 3-D density model of Mt. Etna volcano (Southern Italy). J Volcanol Geotherm Res 164:161–175

Spilliaert N, Allard P, Métrich N, Sobolev AV (2006) Melt inclusion record of the conditions of ascent, degassing, and extrusion of volatile-rich alkali basalt during the powerful 2002 flank eruption of Mount Etna (Italy). J Geophys Res 111, B04203. doi:10.1029/2005JB003934

Stormer JC, Nicholls J (1978) XLFRAC a programme for interactive testing of magmatic differentiation models. Comp Geosci 4:143–159

Sturiale C (1970) La singolare eruzione dell'Etna del 1763 "La Montagnola". Boll Mineral Rend Soc Ital Mineral Petrol 26:314–351

Tanguy JC, Kieffer G (1977) The 1974 eruption of Mount Etna. Bull Volcanol 40(4):239–252. doi:10.1007/BF02597566

Tibaldi A, Corazzato C, Marani M, Gamberi F (2009) Subaerial-submarine evidence of structures feeding magma to Stromboli Volcano, Italy, and relations with edifice flank failure and creep. Tectonophysics 469:112–136

Viccaro M, Ferlito C, Cortesogno L, Cristofolini R, Gaggero L (2006) Magma mixing during the 2001 event at Mount Etna (Italy): effects on the eruptive dynamics. J Volcanol Geotherm Res 149:139–159

Viccaro M, Ferlito C, Cristofolini R (2007) Amphibole crystallization in the Etnean feeding system: mineral chemistry and trace element partitioning between Mg-hastingsite and alkali basaltic melt. Eur J Mineral 19:499–511. doi:10.1127/0935-1221/2007/0019-1747

Viccaro M, Giacomoni PP, Ferlito C, Cristofolini R (2010) Dynamics of magma supply at Mt. Etna volcano (Southern Italy) as revealed by textural and compositional features of plagioclase phenocrysts. Lithos 116:77–91

Villaseñor A, Benz HM, Filippi L, De Luca G, Scarpa R, Patanè G, Vinciguerra S (1998) Three-dimensional P-wave velocity structure of Mt. Etna, Italy. Geophys Res Lett 25(11):1975–1978. doi:10.1029/98GL01240